Time-coded neurotransmitter release at excitatory and inhibitory synapses

Serafim Rodrigues[a,1], Mathieu Desroches[b,1], Martin Krupa[b,1], Jesus M. Cortes[c,d], Terrence J. Sejnowski[e,f,g,2], and Afia B. Ali[h,1]

[a]School of Computing and Mathematics, Plymouth University, Plymouth PL4 8AA, United Kingdom; [b]Inria Sophia Antipolis Mediterranee Research Centre, MathNeuro Team, 06902 Sophia Antipolis cedex, France; [c]Biocruces Health Research Institute, Cruces University Hospital, 48903 Barakaldo, Bizkaia, Spain; [d]Departamento de Biologia Celular e Histologia, University of the Basque Country, 48940 Leioa, Bizkaia, Spain; [e]The Computational Neurobiology Laboratory, Salk Institute, La Jolla, CA 92037; [f]Howard Hughes Medical Institute, Salk Institute, La Jolla, CA 92037; [g]Division of Biological Science, University of California, San Diego, La Jolla, CA 92093; and [h]UCL School of Pharmacy, Department of Pharmacology, University College London, London WC1N 1AX, United Kingdom

Contributed by Terrence J. Sejnowski, December 30, 2015 (sent for review January 1, 2015; reviewed by Antoni Guillamon and Misha Tsodyks)

Communication between neurons at chemical synapses is regulated by hundreds of different proteins that control the release of neurotransmitter that is packaged in vesicles, transported to an active zone, and released when an input spike occurs. Neurotransmitter can also be released asynchronously, that is, after a delay following the spike, or spontaneously in the absence of a stimulus. The mechanisms underlying asynchronous and spontaneous neurotransmitter release remain elusive. Here, we describe a model of the exocytotic cycle of vesicles at excitatory and inhibitory synapses that accounts for all modes of vesicle release as well as short-term synaptic plasticity (STSP). For asynchronous release, the model predicts a delayed inertial protein unbinding associated with the SNARE complex assembly immediately after vesicle priming. Experiments are proposed to test the model's molecular predictions for differential exocytosis. The simplicity of the model will also facilitate large-scale simulations of neural circuits.

SM complex | exocytotic-endocytotic cycle | short-term synaptic plasticity | SNARE complex | asynchronous neurotransmitter release

Molecular and electrophysiological data have revealed differences in the regulation of presynaptic exocytotic machinery, giving rise to multiple forms of neurotransmitter release: synchronous release promptly after stimulation, delayed asynchronous release, and spontaneous release. Synchronous release is induced by rapid calcium influx and, subsequently, calcium-mediated membrane fusion (1). Asynchronous release occurs only under certain conditions (1, 2). Finally, spontaneous mini-releases occur in the absence of action potentials (2).

Two distinct mechanisms have been proposed to explain the various modes of exocytosis. One view suggests distinct signaling pathways and possibly independent vesicle pools (3, 4). The second and more parsimonious view argues that the three modes of release share key mechanisms for exocytosis, specifically, the canonical fusion machinery that operates by means of the interaction between the SNARE attachment protein receptor proteins and Sec1/Munc18 (SM) proteins (5–10) (Fig. 1). The SNARE proteins syntaxin, 25-kDa synaptosome-associated protein (SNAP-25), and vesicle-associated membrane protein (VAMP2; also called synaptobrevin 2), localized on the plasma membrane and the synaptic vesicle, bind to form a tight protein complex, bridging the membranes to fuse.

The canonical building block forms a substrate from which the three release modes differentially specialize with additional regulatory mechanisms and specific Ca^{2+} sources(s) and sensor(s) that trigger the exocytosis cycle. Calcium sensors for synchronous release have been identified as synaptotagmin (e.g., Syt1, Syt2, Syt9). In contrast, the biomolecular processes generating asynchronous and spontaneous release remain unclear and controversial. However, experiments suggest multiple mechanistically distinct forms of asynchronous release operating at any given synapse, and these forms have been associated, for example, with vesicle-associated membrane protein 4 (VAMP4), synaptotagmin (Syt7), double C2 domain protein (Doc2) (still controversial), Rab3-interacting molecules (RIM) proteins, phosphoprotein isoforms synapsin (Syn I and Syn II), and endocannabinoids (eCBs) (11–16). These views are still being debated due to fragmentary and conflicting data (reviewed in 17). In addition, synaptic molecular machinery regulates short-term synaptic plasticity (STSP); however, it is unclear how the molecular mechanisms underlying STSP and exocytotic-endocytotic release are integrated (18).

The present study proposes a semiphenomenological multiple-time-scale model to explain the three modes of release as well as STSP in a unified framework. The model is derived via mass action laws and is based on the biological parsimonious view point pioneered, in particular, by Thomas Südhof (19) (a summary of the key points of the hypothesized biological model and the detailed derivations of the mathematical equations, which rests upon the assumptions of the biological model, is provided in *SI Appendix*). The resulting multiple-time-scale mathematical model describes the canonical SNARE and SM protein interaction exocytotic cycle at a mesoscopic scale, and therefore bridges the gap between molecular protein interactions and electrical synaptic activity, as observed in synaptic dual whole-cell recordings.

Significance

Neurotransmitter exocytosis and short-term synaptic plasticity (STSP) regulate large-scale brain electrical activity. This study is the first, to our knowledge, proposing a multiple-time-scale model that bridges between the microscopic and mesoscopic scales. It is parsimonious, yet with enough descriptive power to express, on the one hand, the interactions between the SNARE and Sec1/Munc18 (SM) protein complexes mediating all forms of neurotransmitter release and STSP and, on the other hand, the electrical activity required for neuronal communication. A key finding is the discovery of a mathematical structure, termed activity-induced transcritical canard, which quantifies and explains delayed and irregular exocytosis. This structure also provides a previously unidentified way to understand delayed and irregular processes sensitive to initial conditions across various biology processes.

Author contributions: S.R., M.D., M.K., T.J.S., and A.B.A. designed research; S.R., M.D., M.K., and A.B.A. performed research; S.R., M.D., M.K., J.M.C., T.J.S., and A.B.A. analyzed data; and S.R., M.D., M.K., J.M.C., T.J.S., and A.B.A. wrote the paper.

Reviewers: A.G., Universitat Politècnica de Catalunya; and M.T., Weizmann Institute of Science.

The authors declare no conflict of interest.

[1]S.R., M.D., M.K., and A.B.A. contributed equally to this work.

[2]To whom correspondence should be addressed. Email: terry@salk.edu.

This article contains supporting information online at www.pnas.org/lookup/suppl/doi:10.1073/pnas.1525591113/-/DCSupplemental.

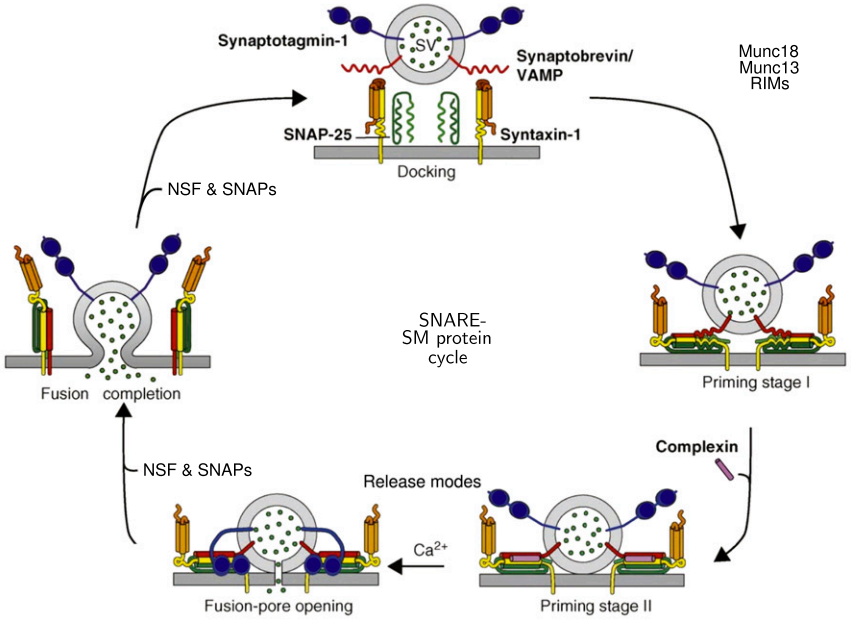

Fig. 1. Parsimonious SNARE-SM molecular exocytotic machinery (modified from ref. 1). Synaptic vesicles, docked at the active zone of a presynaptic terminal, are primed for release by partial SNARE complex assembly that is catalyzed by Munc18, Munc13, and RIMs (*Top*). The second stage involves "superpriming" due to the regulation of complexins on the assembled SNARE complexes, which gives rise to priming stage II. The primed vesicle forms a substrate for either calcium-triggered release via mediation of a calcium sensor, such as synaptotagmins, or spontaneous release, which then enables fusion-pore opening and neurotransmitter release. Subsequently, *N*-ethyl-maleimide–sensitive factor (NSF) and SNAPs mediate disassembly of the SNARE complex, leading to vesicle recycling.

SNARE-SM Model Assembly

To circumvent the prohibitive complexity of modeling all proteins and detailed (as well as unknown) protein interactions involved in the exocytotic process, we propose to model the interaction of protein complexes semiphenomenologically via first principles of mass action, that is, from a mesoscopic view point. In addition, in an attempt to reduce the time complexity of the physiological processes, the model is based on principles from nonlinear dynamics and multiple-time-scale dynamical systems theory (20–23). This approach results in a deterministic 2D model, with variables (p_1, p_2) describing the interactions between the canonical SNARE and SM protein complexes; hence, the name SNARE-SM model (*SI Appendix*). The remaining known exocytotic proteins are considered as regulatory processes, and therefore are treated as parameters that can be tuned to obtain the different modes of release, as idealized in Fig. 2.

There are numerous regulatory proteins; however, only certain proteins are expressed at any given type of synapse (e.g., in Fig. 2, VAMP4 and Syt7 may not be expressed simultaneously). This diversity suggests lumping certain proteins into a single mesoscopic parameter. In contrast, proteins that are shared between different release modes (e.g., Syt1, Syt2, complexin, RIMs, Doc2, TRPV1, voltage-gated Ca^{2+} channel) remain ungrouped. Altogether, nine parameters are associated with the regulatory proteins (model derivation for further biophysical interpretation of the model's parameters is provided in *SI Appendix*).

An important regulatory parameter is the positive small parameter $0 < \varepsilon \ll 1$, which induces a separation of time scales between p_1 and p_2. Specifically, p_1 corresponds to a slow-acting protein complex, whereas p_2 is a fast-acting protein complex. The remaining parameters regulate the interaction strength between p_1 and p_2 as well as the conformational changes of the individual protein complexes. The resulting model expresses features of slow, evoked irregular and spontaneous activation. These features emerge from the rules of interaction between the protein complexes (p_1, p_2) as expressed by the right-hand side of the SNARE-SM model equations (*SI Appendix*). These interactions are best described (in mathematical terms) by plotting the components of the interaction rules (technically, nullclines) in a 2D space (phase-space) spanned by the actions of p_1 and p_2 (Fig. 3*A* and

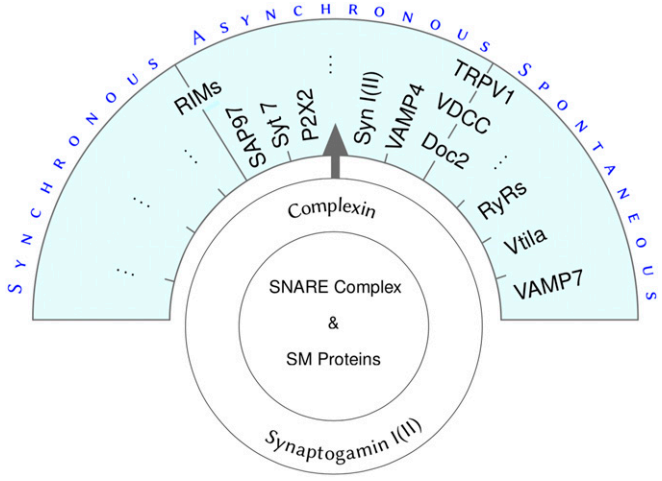

Fig. 2. Schematic idealization of the SNARE-SM model. The circular center describes the canonical fusion machinery constituted by the SNARE complex and SM proteins, which is ultimately regulated by complexin and synaptogamins (19). This building block is signaled by various proteins and, depending on the proteins involved, the appropriate neurotransmitter release mode is activated (i.e., synchronous, asynchronous, spontaneous). Some of the known proteins associated with each type of release are indicated (reviewed in 17, including a complete description and the latest view on the association between proteins and release modes). The RIM proteins are shared between synchronous and asynchronous release modes, whereas TRPV1, Doc2, and voltage-gated Ca^{2+} channels (VDCCs) are shared between asynchronous and spontaneous release modes. The remaining proteins are specific to each release mode; however, inhibiting a protein specific to a given release mode will favor the expression of other modes (17).

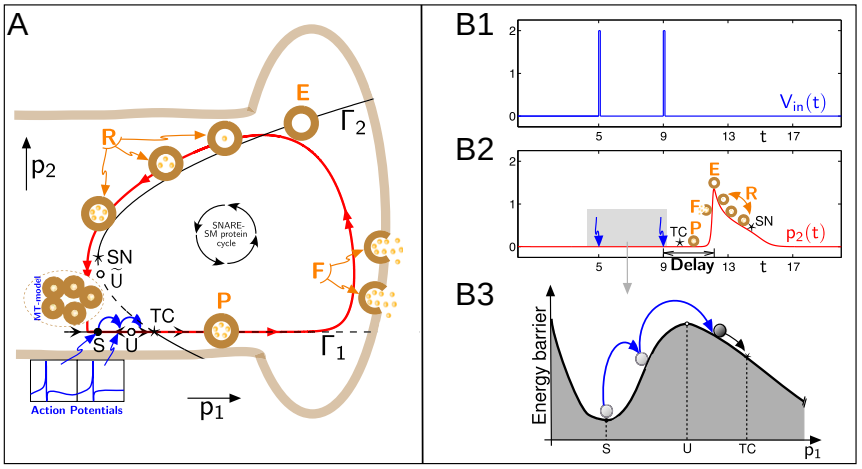

Fig. 3. SNARE-SM model dynamics and asynchronous mechanism. (*A*) Interactions between protein complexes p_1 and p_2 along the vesicle cycle are given by the parabola and the horizontal line (black). These interactions give rise to special points S, U, TC, and SN, which mediate all of the functions associated with the exocytotic-endocytotic cycle (red curve): priming (P), fusion (F), endocytosis (E), and refilling (R). Note that priming stage I initiates after point U, whereas priming stage II initiates after point TC. Arrows indicate dynamic trajectories in the phase plane. Time course of presynaptic voltage (*B1*) and p_2 activity following a stimulus (*B2*). Note that, here, *t* refers to a dimensionless time. (*B3*) Schematic diagram of an energy landscape where stimulus spikes are required to activate p_1 and p_2, represented as a particle that initiates movement only if sufficient energy is provided to traverse the energy barrier (U).

SI Appendix, Fig. S1*C*). In particular, the interaction between p_1 and p_2 gives rise to special configuration points of the dynamical system, namely, S (stable equilibrium), U (unstable equilibrium of saddle type), SN (saddle-node point), and TC (transcritical point) (Fig. 3*A* and *SI Appendix*, Fig. S1*C*), which generate all of the functions associated with each stage of the exocytosis-endocytosis cycle.

In particular, S can be associated with Munc13-1, forming a homodimer that inhibits priming. Then, U can be related to the action of Munc13 gating the transition from the closed-syntaxin/Munc18 complex to the SNARE complex formation. Subsequently, TC can be linked to the action of complexin, and, finally, SN can be connected to the refilling of the vesicle pool. It is noteworthy to observe that the resulting phase-space geometry of the mathematical model shares a great deal of similarity with the schematic diagram of the SNARE-SM biological model by Südhof (19) (compare Fig. 3*A* and *SI Appendix*, Fig. S1*C* with *SI Appendix*, Fig. S1*A*). Moreover, the model variables can be activated by a presynaptic stimulus (e.g., calcium influx), represented by the variable $V_{in}(t)$. By means of control parameters, the three modes of neurotransmitter release are mathematically translated into the model's dynamic repertoire: excitability, delayed response to input stimuli, or limit-cycle dynamics (*SI Appendix*). Importantly, the SNARE-SM model is sensitive to initial conditions without generating chaos. This sensitivity constitutes the core mechanism that governs the irregular activation. Furthermore, due to the time scale separation between p_1 and p_2, the delayed neurotransmitter release results from the protein–protein binding and subsequent unbinding that occurs with inertia.

The delay is specifically explained by a previously unexplored mathematical structure that acts as a dynamic (delayed) response to an input via transcritical canards (22, 23), which we denote, "activity-induced transcritical canards" (*SI Appendix*). This structure quantifies the delay and predicts a delayed inertial protein unbinding associated with the SNARE complex assembly immediately after vesicle priming. Previous modeling attempts introduced stochastic elements or a hardwired delay into the model to account for asynchronous release (24–28). In contrast, the delay in the SNARE-SM model emerges as a result of a dynamic mechanism that resembles a biological process.

In brief, the SNARE-SM model has a mechanistic interpretation because it can be related to processes associated with exocytotic-endocytotic signaling pathways, including intracellular calcium dynamics. Moreover, the delayed irregular activation can be associated, for example, with the action of complexin or Syn I(II) and with the presence of eCB, VAMP4, or even Doc2 in the case of excitatory neurons.

Extended SNARE-SM Model. We extend the SNARE-SM model to show how STSP mechanistically integrates within the exocytotic-endocytotic machinery, and also to enable comparison with electrophysiological data. This extension is achieved by feeding the exocytotic-endocytotic signal of the SNARE-SM model into an STSP model, which effectively activates the vesicle pool. In particular, we use the Markram–Tsodyks (MT) STSP model (29–31) (*SI Appendix*). The MT equations phenomenologically model the time evolution of available resources (vesicles) and how efficiently neurotransmitters are released. In the model there are two quantities, namely, the number of vesicles, d, and the release probability, f, which are updated for every presynaptic spike occurring at time instant t_s. The model predicts the amount of neurotransmitter released, $T(t_s) = d(t_s)f(t_s)$, which, in reality, is released with a small time delay.

The MT model successfully accounts for the highly heterogeneous STSP dynamics across different brain areas in the context of synchronous release (table S1 of ref. 31). Consequently, the proposed model extends the MT model by incorporating all three modes of neurotransmitter release observed at unitary synapses. However, to complete the model framework and to enable testing against data sampled from whole-cell paired recordings obtained from unitary synapses, an observational variable representing postsynaptic potentials is required. This observational variable is modeled with the standard conductance-based (subthreshold) equation, where the action of neurotransmitters on postsynaptic neurotransmitter receptors follows the first-order kinetic equation (*SI Appendix*). More detailed approaches for modeling receptor dynamics [e.g., detailed kinetics (32)] will be a matter for future consideration.

Results

SNARE-SM Model Dynamics. The SNARE-SM model has three operating modes. Fig. 3*A* shows a presynaptic terminal, which encloses the SNARE-SM model's signaling mechanism. The black arrows labeled p_1 and p_2 span the 2D space within which the protein complexes interact. This space is not physical, but

rather a phase-space where protein functions take place and the values of p_1 and p_2 represent the levels of activity between protein complexes. The line Γ_1 and the parabola Γ_2, called the fast nullclines, indicate the regions in which the functions of the protein complexes are quasistationary (Fig. 3*A* and *SI Appendix*, Fig. S1*C*). The line Γ_1 is stable to the left of the transition point TC, and the parabola Γ_2 is stable above the transition point SN. Past the transition points, the fast nullclines become unstable (Fig. 3*A* and *SI Appendix*, Fig. S1*C*, dashed lines). For clarity, the slow nullclines are not displayed (*SI Appendix*).

The stability of the fast nullclines is assessed by looking at the mathematical limit of the model when p_1 is kept constant ($\varepsilon = 0$) (details are provided in *SI Appendix*). In this limit, the only variable left is p_2, and p_1 acts as a parameter; the equilibrium states lie on the fast nullclines, and their stability depends on the parameter p_1 and change at bifurcation points SN and TC. Under normal operating conditions ($\varepsilon > 0$), p_1 evolves slowly; the points SN and TC are not bifurcation points of the model any longer; however, they still organize dynamic transitions between different levels of quasistationary activity close to Γ_1 and Γ_2. Moreover, the SNARE-SM model possesses two true stationary states, marked S and U (Fig. 3*A* and *SI Appendix*, Fig. S1*C*), which endow it with an excitable structure.

An exocytotic signal (Fig. 3*A*, red trajectory) is evoked by one or more presynaptic spikes. Input stimuli excite the system away from the functionally inactive state S. However, the protein complexes switch their functional behavior past the switching point (U) only when sufficient energy is available, via action potentials and an increase in calcium influx. In this case, the system passes the TC transition point, which enables the appropriate exocytotic signaling mode to be activated. Fig. 3*B* illustrates the process in the time domain: Fig. 3*B1* shows the presynaptic stimulus; Fig. 3*B2* shows the output signal; and Fig. 3*B3* is a schematic diagram that depicts a particle (in the abstract sense), initially at a rest point (S), that is driven out of the basin of attraction of S by a sufficient force (blue arrows), enabling it to jump the energy barrier (U). We refer the reader to the article by Kasai et al. (33) for discussion on energy functions associated with the release of neurotransmitters. Thus, a particular amplitude and timing of a perturbation can drive the system away from the equilibrium point and induce it to make a large-amplitude, transient excursion before it settles again to its inactive state (S).

Past the switching point (U), the protein complexes p_1 and p_2 begin to interact strongly, activating states associated with vesicle priming I. The passage through the TC point can be associated with the initiation of priming stage II (i.e., SNARE complex assembly and regulation by complexin). Priming can be a fast (synchronous) or slow (asynchronous) process, depending on the time scale parameter ε.

From a mathematical perspective, precise quantitative control of the delay is achieved by the so-called "way-in–way-out function" (*SI Appendix*). In short, the activity-induced transcritical canard predicts the existence of delayed inertial protein unbinding occurring between priming I and fusion-pore opening stages. This delayed inertial protein unbinding can possibly be related to the clamping action of complexin, or Ca^{2+}-activated calcium sensors (e.g., Syt1) competing with complexin for SNARE complex binding (by displacing part of complexin within the SNARE but via a delayed inertial unbinding). Indeed, from the modeling point of view, ε (which also controls the delayed process), can be associated with complexin or (a)synchronous calcium sensors at a molecular level (*SI Appendix*). The unbinding between p_1 and p_2 (e.g., interpreted mesoscopically as translocation of complexin) initiates fusion (F) and subsequent neurotransmitter release. Following exocytosis, p_1 and p_2 begin a second phase of strong interaction that induces endocytosis (E) and subsequent vesicle refilling (R). The final stage is triggered by the SN transition point, which prompts p_1 and p_2 to alter their states and evolve toward their inactive state S, where the vesicle pool is replenished.

SNARE-SM Model Evoked Release Mode. Evoked synchronous and asynchronous modes of release in the SNARE-SM model are shown in *SI Appendix*, Figs. S2 and S3, with the parameters specified in *SI Appendix*, Table S1. For the synchronous mode, *SI Appendix*, Fig. S3 *A–A2* shows that the SNARE-SM model's output, p_2, is activated almost instantaneously upon an incoming stimulus, V_{in}. In this case, ε has a small value. Increasing ε induces a weaker binding/unbinding that effectively introduces variability (irregular activation via sensitivity to initial conditions) and a strong inertia in the unbinding process, causing a delay. This asynchronous mode is shown in *SI Appendix*, Fig. S3 *B–B2*, where the onset of p_2 is delayed with respect to the stimulus. Note that the output time profile also changes shape and amplitude, with a slower rising phase. These features are crucial, leading to gradual activation of vesicle pools as well as postsynaptic receptors, consistent with the gradual postsynaptic potential response observed in experiments for asynchronous release (1).

SI Appendix, Fig. S2 shows three different delayed responses under the same two-spike stimulus, demonstrating irregular activation due to the model's sensitivity to initial conditions. Moreover, a burst of spikes may be required before the vesicle pool is activated, a feature that is widely reported in experiments (1); this burst of spikes is controlled by increasing the distance between the two configuration states S and U, thereby increasing the energy barrier (Fig. 3*B3*). The farther they are apart, the stronger is the stimulus (multiple spikes) that is needed to elicit vesicle priming (P). A delayed response to a stimulus with three spikes is shown in *SI Appendix*, Fig. S3 *C–C2*). Note that if the interspike interval between input stimuli is smaller than the exocytotic-endocytotic cycle time, then the delay decreases inversely to the input frequency increase. However, this delay does not decrease below a fixed value that corresponds to synchronous release.

SNARE-SM Model Spontaneous Release Mode. There are two different ways to generate spontaneous mini-releases in the SNARE-SM model as illustrated in *SI Appendix*, Fig. S4 *A–B1*, respectively. One way is to assume that Ca^{2+} channels open stochastically, which changes the resting baseline of Ca^{2+} concentrations (2). Increasing the Ca^{2+} concentration decreases the amplitude of the parabola Γ_2, which changes the fusion dynamics. This change can be related to empirical data showing the existence of multiple fusion processes, such as kiss-and-run, clathrin-dependent endocytosis, and bulk endocytosis (34). Kiss-and-run is relevant to spontaneous release, where vesicles do not fuse entirely with the membrane, and thus are rapidly retrieved from the active zone (release site).

The model also needs to be in a strongly excitable regime, in which the two configuration states S and U are sufficiently close to each other. As a consequence, low-noise perturbations are sufficient to kick the system away from its inactive state (S) to complete endocytosis before settling back to S (*SI Appendix*, Fig. S4*B1*). An alternative mode of spontaneous release is via Ca^{2+} sparks from internal Ca^{2+} stores (1, 2), which stimulates a limit cycle (a self-sustained periodic signal) (*SI Appendix*, Fig. S4*A1*) that is achieved by moving both the S and U configuration points to the far left; as a consequence, signals emanating from the SN point no longer fall into the basin of attraction of S, prompting another exocytotic-endocytotic cycle. The limit cycle can have an irregular period by random variation of its associated parameters (*SI Appendix*).

Extended SNARE-SM Model Predictions. We now test the full model [extended (E)-SNARE-SM] with paired whole-cell recordings from both inhibitory and excitatory synapses having differential modes of exocytosis. For inhibition, we use recordings from isolated synapses between cholecystokinin (CCK)-positive Shaffer collateral-associated

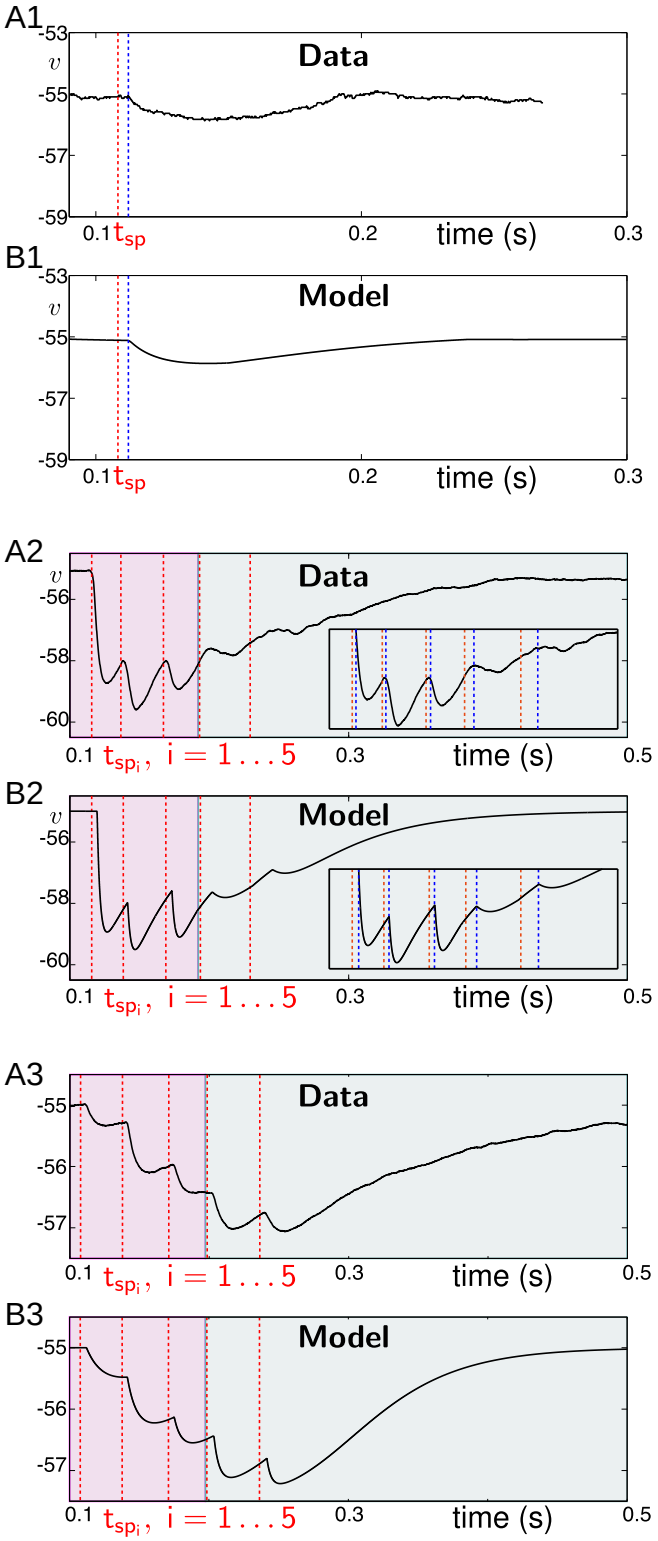

Fig. 4. Model comparison with inhibitory synapse. (*A1*) Delayed IPSP (~5.6 ms) of CCK-positive SCA interneuron to unitary input spike at time t_{sp} (dashed red line). (*B1*) Response of the model to the same input as in *A1*. (*A2*) Depressed and delayed IPSP data resulting from spikes occurring at times t_{sp_i}, $i = \{1 \ldots 5\}$ (red dashed lines). The first epoch (shaded magenta rectangle) is triggered by the first three spikes causing synchronous mode (release within 5 ms); the second epoch (shaded cyan rectangle) is initiated by two subsequent spikes that lead to asynchronous mode (more than 5-ms delayed release). (*Inset*) Expansion of the region corresponding to the five release events: Vertical red dashed lines mark spike times, and vertical blue lines mark IPSP response times. The distance between them measures the delay: ~(2.0, 2.6, 2.5, 9.2, 15.0) ms. (*B2*) Response of the model to the same input as in *A2*. (*A3*) Facilitated and delayed IPSP data. The first epoch (shaded magenta rectangle), induced by the first three spikes, leads to synchronous release with delayed response times of ~(4.2, 3.6, 4.1) ms. The second epoch (shaded cyan rectangle) is evoked by two subsequent spikes, with marginal delayed release times [~(5.0, 5.1) ms]. (*B3*) Response of the model to the same input as in *A3*.

(SCA) interneurons in the CA1 region of P18-21 rat hippocampus (16) (*Materials and Methods*) and we base the model on parameters associated with $GABA_A$-induced currents (16, 35, 36). For excitation, we use data from experiments on calyx-of-Held synapses (4). The SNARE-SM model parameters are adjusted to generate the appropriate release mode (*SI Appendix*, Table S1), and the MT model parameters are adopted from Markram et al. (37) as a baseline (*SI Appendix*). Note that asynchronous release is known to be accompanied by irregularity in both neurotransmitter release times and amplitudes of the inhibitory postsynaptic potentials (IPSPs) and excitatory postsynaptic potentials; therefore, associated parameter values can vary substantially between release events. The remaining parameters are tuned within a bounded region (inhibitory synapses are shown in *SI Appendix*, Table S2, and excitatory synapses are shown in *SI Appendix*, Table S3). Details of the parameter fitting procedures are provided in *SI Appendix*.

The E-SNARE-SM model successfully reproduces the synaptic dynamics of the SCA inhibitory synapse (Fig. 4). The delayed unitary IPSP in Fig. 4*A1* is compared with the output of the inhibitory model (Fig. 4*B1*). A sequence of IPSPs exhibiting short-term synaptic depression and delay in response to multiple presynaptic stimuli (Fig. 4*A2*) matches the output of the model in Fig. 4*B2*. The response to a sequence of IPSPs featuring short-term synaptic facilitation and delay, shown in Fig. 4*A3*, is compared with the response of the model in Fig. 4*B3*. The model reproduces the onset of the delays and the temporal profile of the IPSP data. Care was taken with fitting delayed release because the model is sensitive to initial conditions. Completion of an exocytotic-endocytotic cycle brings the system to a different configuration. As a consequence, the parameters of the previous exocytotic-endocytotic cycle will give rise to a different delayed response when a new stimulus occurs. Parameters associated with $GABA_A$-induced currents also undergo changes, albeit minor, because eCBs increase the input resistance of the cell, docking time of neurotransmitters, and affinity.

The parameters of the MT model also depend on the mode of release. Continuity conditions are enforced to ensure that different epochs of data fit with different modes of release (shaded magenta and cyan rectangles in Fig. 4 *A2*, *B2*, *A3*, and *B3*). Future developments will include the conditions ensured by the way-in–way-out function for an automatic parameter fitting. However, in the limit of complete depletion of neurotransmitters, fitting any continuous mesoscopic model to electrophysiological data becomes increasingly difficult, because noise dominates and expressing microscopic dynamics becomes fundamental (averaging effect is shown in *SI Appendix*, Fig. S7). In this limit, other theoretical studies reveal that discrete, stochastic, or agent-based models best describe microscopic activity (38).

Comparisons between excitatory postsynaptic currents at the calyx-of-Held synapse and the postsynaptic currents of the E-SNARE-SM model are made in Fig. 5. Specifically, Fig. 5*A1* depicts a synchronous activation to a single presynaptic spike, which is matched by the model in Fig. 5*B1*. Multiple postsynaptic activations elicited by a single input are shown in Fig. 5*A2*. The first postsynaptic activation is asynchronous, and the two subsequent releases are spontaneous. The model is in good agreement over three epochs shown in different colors (Fig. 5*B2*). Moreover, the model can also reproduce the WT data from the calyx of Held.

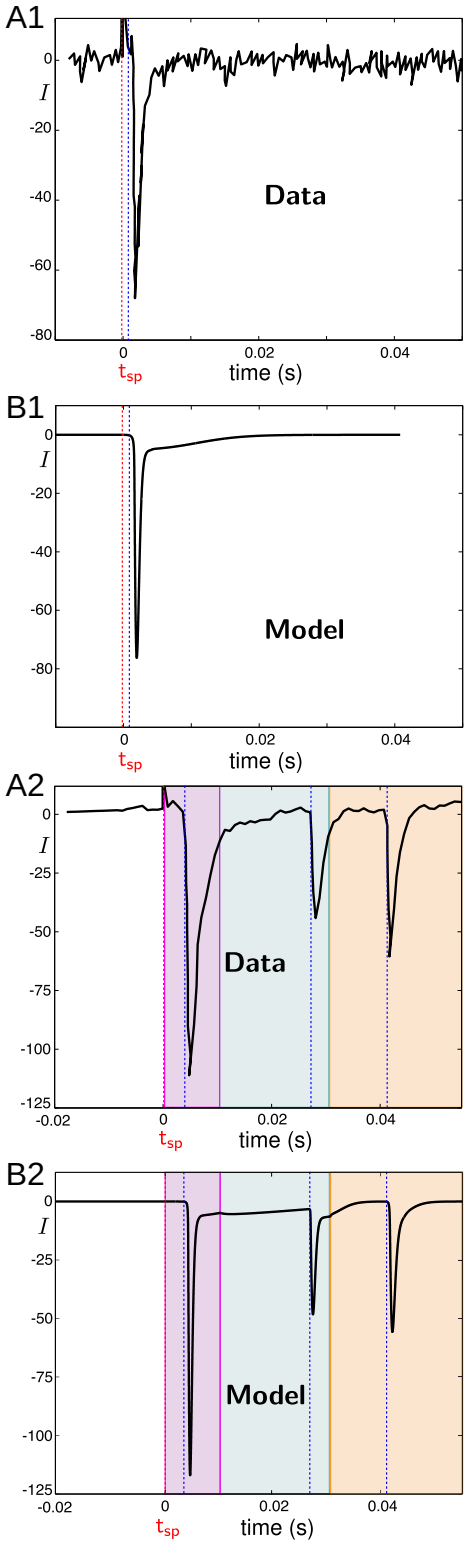

Fig. 5. Model comparison with excitatory synapse. (*A1*) Synchronous excitatory postsynaptic current (EPSC; at ∼1.6 ms) of the calyx-of-Held synapse to unitary input spike at time t_{sp} (dashed red line). The blue dashed line shows the time instant of activation. Data were extracted from figure 2A of ref. 4 (Syt2 KO). (*B1*) Response of the model to the same input as in *A1*. (*A2*) Unitary input spike at time t_{sp} (dashed red line) first causes a delayed EPSC (at ∼4 ms) and two additional spontaneous activations at ∼(27.3, 41.3) ms. Data were extracted from figure 2A of ref. (4) (Syt2 KO). (*B2*) Response of the model to the same input as in *A2*. Here, the different epochs of the data reflect the transitions from delayed (shaded magenta rectangle) to spontaneous (shaded cyan and shaded light orange rectangles) activation. The model makes these transitions by varying the parameters of the SNARE-SM model that dictate the transition from the delayed to spontaneous regime (*SI Appendix*, Table S1).

In particular, the strong synaptic depression seen at this synapse during high-frequency stimulation and the kinetics of recovery from synaptic depression can both be captured. Indeed, our model builds upon the MT framework, which has been shown to account for these phenomena (39).

Discussion

The proposed multiple-time-scale SNARE-SM model extends the MT framework for STSP by incorporating all three forms of exocytosis at the same mesoscopic level of description (37). Moreover, our mathematical model is in good agreement with the biological SNARE-SM model of Südhof (19) (compare again Fig. 3 and *SI Appendix*, Fig. S1*C* with *SI Appendix*, Fig. S1*A*). Details of the biochemical pathways involved in exocytosis are semiphenomenologically expressed; therefore, predictions of the model can be compared with SNARE-SM physiology, and computational hypotheses can be explored to propose novel experiments. For example, in the model, the three distinct forms of release share the same exocytotic machinery, where the modes of exocytosis are a consequence of parameters in the model. Therefore, in every exocytosis-endocytosis cycle, the release mode may switch due to slowly varying physiological variables that have not yet been identified. However, it is important to be cautious because there may be different vesicle pools or pathways (e.g., different calcium sensors) (4).

The time-scale parameter ε modulates the activity-induced transcritical canard, which mechanistically explains the ratio between synchronous and asynchronous release. The way-in–way-out function quantifies how the exocytotic-endocytotic signaling pathway fine-tunes the timing of neurotransmitter release, which can be seen as a homeostatic mechanism for efficient neuronal communication. This mechanism is consistent with molecular studies showing that within the canonical fusion machinery, Syt1 and complexin are functionally interdependent and are potentially the key players in regulating all modes of release (19). Specifically, Syt1 mediates calcium-triggered release and controls the rate of spontaneous release (i.e., speed and precision of release by associations with SNARE complexes). Complexin is a cofactor for Syt1 that functions both as a clamp and as an activator of calcium-triggered fusion (19).

Further upstream, other proteins could signal (via yet unknown interactions) this homeostatic system. For example, studies show that Syn I(II), known to coat synaptic vesicles and to have a postdocking role, regulates synchronous and asynchronous release (15). In particular, Syn II interacts directly with P/Q type and indirectly with N-type Ca^{2+} channels to increase asynchronous release. Additionally, Syn I(II) seems to constitute a push/pull mechanism regulating the ratio between synchronous and asynchronous release (15), thus suggesting that they share exocytotic mechanisms. Deeper insight into this mechanism could result from further molecular studies investigating the existence of a signaling pathway between cannabinoid type 1 (CB1) receptor, Syn I(II), RIMs, and RIM-BS proteins, because CB1 also appears to interact with N-type and P/Q-type Ca^{2+} channels (40, 41). Nevertheless, multiple exocytotic mechanisms should not be ruled out, and augmenting the proposed model to allow switching between them is a focus for future research.

The proposed model could also be mapped onto the dual calcium-sensor model (4). Another reported mechanism that should be considered is the VAMP4-enriched vesicle pool, which

is formed after intense stimulation and enables asynchronous release (11). Surprisingly, the authors show that VAMP4-driven SNARE complexes do not readily interact with synaptotagmin and complexin, which challenges the widely held view that synchronous release requires interaction of SNARE complexes (e.g., VAMP4/SNAP-25, syntaxin-1) with Syt1 and complexins. This issue could be resolved by seeking an alternative way to elicit VAMP4-mediated release (identifying a different signaling pathway). In view of the present model, it would be relevant to test for VAMP4 in synapses expressing CCK. Despite these observations, the SNARE-SM model can explain these results without assuming the existence of a second, VAMP4-enriched pool of vesicles (*SI Appendix*, Fig. S5 *B–B2*). Another refinement may emerge from a recent study showing that 2-arachidonoyglycerol (2-AG)/anandamide directly modulates $GABA_A$ postsynaptic receptors, therefore affecting neurotransmitter docking times and possibly contributing to asynchronicity (42). Other forms of synaptic plasticity, such as spike timing-dependent plasticity mediated by differential exocytosis, could also be explored with the proposed model (*SI Appendix*, Fig. S6).

Finally, the SNARE-SM model will facilitate large-scale network simulations and consequently explain the functional role of differential exocytosis and synaptic plasticity on network states underlying memory, cognition, and pathological brain states (e.g., epilepsy) (43). At a microscale, the proposed theoretical approach could provide new insights into the function of other protein–protein interactions. For example, activity-induced transcritical canards can explain recent experiments that identify proteins mediating the asynchronous activation of sodium and potassium channels (44).

Materials and Methods

Inhibitory Synapses.

Experimental preparations and observations. The data are sampled from paired whole-cell recordings obtained from unitary synapses between CCK-positive SCA interneurons in the CA1 region of P18–P21 rat hippocampus (45) (*SI Appendix*, Fig. S7). These cells possess a modulatory feedback mechanism that allows the postsynaptic cell to control the level of presynaptic $GABA_A$ release via the eCB system, which is composed of cannabinoid receptors, ligands, and the relevant enzymes (45). Specifically, eCB, 2-AG, or anandamide is synthesized and released on demand, involving depolarization of the postsynaptic membrane via the activation of voltage-dependent L-type calcium channels (46). Once synthesized, it diffuses across the synaptic cleft to modulate the activation of CB1 receptors located in the presynaptic cell. Subsequently, CB1 receptors inactivate N-type (and possibly P/Q-type) calcium channels (therefore reducing Ca^{2+} concentration) leading to a reduction of $GABA_A$ release (45). Experimentally, the level of CB1 receptor activation and deactivation was controlled by bath application of endogenous agonist, anandamide, and antagonist AM-251. The endogenous agonist effects could be mimicked by depolarization-induced suppression of inhibition protocols, which involved depolarization of the postsynaptic membrane (45). These modulatory synaptic effects have a direct impact on the timing of synaptic inhibition, specifically asynchronous release and STSP (*SI Appendix*, Fig. S7). Details of the experimental preparation are explained.

Slice preparation. Male Wistar rats (P18–P23; Harlan UK) were anesthetized with sodium pentobarbitone (60 mg/kg Euthatal; Merial) via i.p. injection and perfused transcardially with ice-cold modified artificial cerebral spinal fluid (ACSF) containing 15 mM D-glucose, 248 mM sucrose, 2.5 mM $CaCl_2$, 3.3 mM KCl, 1.2 mM $MgCl_2$, 25.5 mM $NaHCO_3$, and 1.4 mM NaH_2PO_4. Following decapitation, the brain was removed and 300-μm-thick coronal slices of cerebral cortex were cut. These procedures were performed under UK Home Office guidelines by authorized Home Office license holders. The severity of the procedures was classed as moderate. The total number of rats used for this study was 61. Slices were incubated for 1 h before recording, for which they were placed in a submerged chamber perfused with ACSF at a rate of 1–2 $mL \cdot min^{-1}$. ACSF contained 20 mM D-glucose, 2 mM $CaCl_2$, 2.5 mM KCl, 1 mM $MgCl_2$, 121 mM NaCl, 26 mM $NaHCO_3$, and 1.25 mM NaH_2PO_4 [equilibrated with 95% (vol/vol) O_2 and 5% (vol/vol) CO_2]. All substances used to make ACSF solutions were obtained from VWR International (45).

Electrophysiological recordings. Electrodes with resistances of 8–11 MΩ were pulled from borosilicate glass and filled with an intracellular solution containing 144 mM K-gluconate, 0.2 mM EGTA, 10 mM Hepes, 3 mM $MgCl_2$, 0.2 mM Na_2-ATP, 0.2 mM Na_2-GTP, and 0.02% (wt/vol) biocytin (pH 7.2–7.4, 300 mOsm). Slices were viewed using videomicroscopy under near-differential interference contrast illumination to enable cells to be chosen based upon the shape of their soma and dendritic projections. Neurons were further identified by their firing properties following a series of 500-ms depolarizing current steps from +0.05 nA to +0.15 nA. Dual whole-cell recordings were performed in a current clamp at room temperature in CA1 stratum radiatum and lacunosum moleculare border. Presynaptic action potentials were generated by a depolarizing current injection of varying length (5–10 ms) to enable IPSPs to be observed in response to single, double, or trains of action potentials. Connections were tested in both directions for all pairs. Data were acquired with SEC 05L/H amplifiers (NPI Electronic GmbH). Recordings were filtered at 2 KHz, digitized at 5 KHz using a CED 1401 interface (Cambridge Electronic Design), and stored on a hard disk drive. Input resistances were continually monitored by injecting a small hyperpolarizing current injection for 20 ms at the start of each frame.

Pharmacology. The endogenous cannabinoid receptor agonist anandamide (14 μM, in water-soluble emulsion) was used. AM-251 [1-(2,4-dichlorophenyl)-5-(4-iodophenyl)-4-methyl-*N*-(1-piperidyl)pyrazole-3-carboxamid; Tocris], a selective CB1 receptor inverse agonist, was dissolved in DMSO, stored as stock at −20 °C, and bath-applied at 10 μM. AM-251 is structurally very close to SR141716A, a cannabinoid receptor antagonist, but it exhibits a higher binding affinity for the CB1 receptor with a K_i value of 7.5 nM compound to SR141716A, which has a K_i value of 11.5 nM.

Electrophysiological data analysis. Using Signal (Cambridge Electronic Design), the electrophysiological characteristics of the recorded cells were measured from their voltage responses to 500-ms current pulses between −0.2 and +0.1 nA in amplitude. Postsynaptic events were either accepted for analysis or rejected. Individual sweeps were observed and accepted, edited, or rejected according to the trigger points that would trigger measurements and averaging of the IPSPs during subsequent data analysis. Averaging of IPSPs was triggered from the rising phase of the presynaptic spike. Apparent failures of synaptic transmission were counted manually, and IPSP amplitudes in the range of the synaptic noise were taken as failures. Selection and averaging of these apparent failures resulted in no measurable postsynaptic responses. Single-sweep IPSP amplitudes were measured from the baseline to the peak of the IPSP and are displayed as ±SD. IPSP half-width and the 10–90% rise time were obtained from averages created from 100 to 300 sweeps. IPSP latencies were manually measured as the time delay between presynaptic action potential peaks to the onset of the detectable IPSPs. The fluctuations in the IPSP latencies were quantified in nonoverlapping time interval sets of 5 ms after each presynaptic action potential. Synchronous release was taken as release of neurotransmitter within 0- to 5-ms latencies, whereas asynchronous release was taken as the release of neurotransmitter falling within a time window of 5- to 15-ms latencies (40). The synchronicity ratio was calculated as the ratio of synchronous release/asynchronous release (from a dataset of 100–300 sweeps).

Excitatory Synapses. Recordings were performed in the laboratory of Thomas Südhof (Stanford University, Stanford, CA). In particular, data in Fig. 4 *A1* and *A2* were extracted from figure 2A of ref. 10 (Syt2 KO).

Software. Electrophysiological data were acquired and analyzed offline using Signal. For model simulations, we used the software package XPPAUT (47). The parameter fitting of the model from data was carried out with MATLAB (MathWorks).

ACKNOWLEDGMENTS. We thank Dr. Thomas Südhof (Stanford University) for providing voltage-clamp recordings of the calyx-of-Held synapses (4). A.B.A. thanks the Medical Research Council (United Kingdom) New Investigators Award for funding the experiments. J.M.C. is funded by Ikerbasque: The Basque Foundation for Science. T.J.S. is supported by the Howard Hughes Medical Institute, NIH, and Office of Naval Research.

1. Pang ZP, Südhof TC (2010) Cell biology of Ca2+-triggered exocytosis. *Curr Opin Cell Biol* 22(4):496–505.
2. Smith SM, et al. (2012) Calcium regulation of spontaneous and asynchronous neurotransmitter release. *Cell Calcium* 52(3):226–233.
3. Sara Y, Virmani T, Deák F, Liu X, Kavalali ET (2005) An isolated pool of vesicles recycles at rest and drives spontaneous neurotransmission. *Neuron* 45(4):563–573.
4. Sun J, et al. (2007) A dual-Ca2+-sensor model for neurotransmitter release in a central synapse. *Nature* 450(7170):676–682.

5. Verhage M, et al. (2000) Synaptic assembly of the brain in the absence of neurotransmitter secretion. *Science* 287(5454):864–869.
6. Schoch S, et al. (2001) SNARE function analyzed in synaptobrevin/VAMP knockout mice. *Science* 294(5544):1117–1122.
7. Bronk P, et al. (2007) Differential effects of SNAP-25 deletion on Ca2+ -dependent and Ca2+ -independent neurotransmission. *J Neurophysiol* 98(2):794–806.
8. Zhou P, et al. (2013) Syntaxin-1 N-peptide and Habc-domain perform distinct essential functions in synaptic vesicle fusion. *EMBO J* 32(1):159–171.
9. Broadie K, et al. (1995) Syntaxin and synaptobrevin function downstream of vesicle docking in Drosophila. *Neuron* 15(3):663–673.
10. Vilinsky I, Stewart BA, Drummond J, Robinson I, Deitcher DL (2002) A Drosophila SNAP-25 null mutant reveals context-dependent redundancy with SNAP-24 in neurotransmission. *Genetics* 162(1):259–271.
11. Raingo J, et al. (2012) VAMP4 directs synaptic vesicles to a pool that selectively maintains asynchronous neurotransmission. *Nat Neurosci* 15(5):738–745.
12. Maximov A, et al. (2008) Genetic analysis of synaptotagmin-7 function in synaptic vesicle exocytosis. *Proc Natl Acad Sci USA* 105(10):3986–3991.
13. Pang ZP, et al. (2011) Doc2 supports spontaneous synaptic transmission by a Ca(2+)-independent mechanism. *Neuron* 70(2):244–251.
14. Calakos N, Schoch S, Südhof TC, Malenka RC (2004) Multiple roles for the active zone protein RIM1α in late stages of neurotransmitter release. *Neuron* 42(6):889–896.
15. Medrihan L, et al. (2013) Synapsin II desynchronizes neurotransmitter release at inhibitory synapses by interacting with presynaptic calcium channels. *Nat Commun* 4:1512.
16. Ali AB (2007) Presynaptic Inhibition of $GABA_A$ receptor-mediated unitary IPSPs by cannabinoid receptors at synapses between CCK-positive interneurons in rat hippocampus. *J Neurophysiol* 98(2):861–869.
17. Kaeser PS, Regehr WG (2014) Molecular mechanisms for synchronous, asynchronous, and spontaneous neurotransmitter release. *Annu Rev Physiol* 76:333–363.
18. Lipstein N, et al. (2013) Dynamic control of synaptic vesicle replenishment and short-term plasticity by Ca(2+)-calmodulin-Munc13-1 signaling. *Neuron* 79(1):82–96.
19. Südhof TC (2013) A molecular machine for neurotransmitter release: Synaptotagmin and beyond. *Nat Med* 19(10):1227–1231.
20. Krupa M, Szmolyan P (2001) Extending slow manifolds near transcritical and pitchfork singularities. *Nonlinearity* 14(6):1473–1491.
21. Desroches M, Krupa M, Rodrigues S (2013) Inflection, canards and excitability threshold in neuronal models. *J Math Biol* 67(4):989–1017.
22. Lobry C (1991) Dynamic bifurcations. *Lecture Notes in Math*, ed Benoît E (Springer, Berlin), Vol 1493, pp 1–13.
23. Benoît E, et al. (1981) Chasse au canard. *The College Mathematics Journal* 32:37–119.
24. Volman V, Gerkin RC, Lau PM, Ben-Jacob E, Bi GQ (2007) Calcium and synaptic dynamics underlying reverberatory activity in neuronal networks. *Phys Biol* 4(2):91–103.
25. Nadkarni S, Bartol TM, Sejnowski TJ, Levine H (2010) Modelling vesicular release at hippocampal synapses. *PLOS Comput Biol* 6(11):e1000983.
26. Volman V, Levine H, Sejnowski TJ (2010) Shunting inhibition controls the gain modulation mediated by asynchronous neurotransmitter release in early development. *PLOS Comput Biol* 6(11):e1000973.
27. Volman V, Gerkin RC (2011) Synaptic scaling stabilizes persistent activity driven by asynchronous neurotransmitter release. *Neural Comput* 23(4):927–957.
28. Nadkarni S, Bartol TM, Stevens CF, Sejnowski TJ, Levine H (2012) Short-term plasticity constrains spatial organization of a hippocampal presynaptic terminal. *Proc Natl Acad Sci USA* 109(36):14657–14662.
29. Markram H, Tsodyks M (1996) Redistribution of synaptic efficacy between neocortical pyramidal neurons. *Nature* 382(6594):807–810.
30. Tsodyks MV, Markram H (1997) The neural code between neocortical pyramidal neurons depends on neurotransmitter release probability. *Proc Natl Acad Sci USA* 94(2):719–723.
31. Wang Y, et al. (2006) Heterogeneity in the pyramidal network of the medial prefrontal cortex. *Nat Neurosci* 9(4):534–542.
32. Raghavachari S, Lisman JE (2004) Properties of quantal transmission at CA1 synapses. *J Neurophysiol* 92(4):2456–2467.
33. Kasai H, Takahashi N, Tokumaru H (2012) Distinct initial SNARE configurations underlying the diversity of exocytosis. *Physiol Rev* 92(4):1915–1964.
34. Danglot L, Galli T (2007) What is the function of neuronal AP-3? *Biol Cell* 99(7): 349–361.
35. Cea-del Rio CA, Lawrence JJ, Erdelyi F, Szabo G, McBain CJ (2011) Cholinergic modulation amplifies the intrinsic oscillatory properties of CA1 hippocampal cholecystokinin-positive interneurons. *J Physiol* 589(Pt 3):609–627.
36. Tricoire L, et al. (2011) A blueprint for the spatiotemporal origins of mouse hippocampal interneuron diversity. *J Neurosci* 31(30):10948–10970.
37. Markram H, Wang Y, Tsodyks M (1998) Differential signaling via the same axon of neocortical pyramidal neurons. *Proc Natl Acad Sci USA* 95(9):5323–5328.
38. Campillo F, Lobry C (2012) Effect of population size in a predator–prey model. *Ecol Modell* 246:1–10.
39. Hermann J, Grothe B, Klug A (2009) Modeling short-term synaptic plasticity at the calyx of Held using in vivo-like stimulation patterns. *J Neurophysiol* 101(1):20–30.
40. Twitchell W, Brown S, Mackie K (1997) Cannabinoids inhibit N- and P/Q-type calcium channels in cultured rat hippocampal neurons. *J Neurophysiol* 78(1):43–50.
41. Ali AB (2011) CB1 modulation of temporally distinct synaptic facilitation among local circuit interneurons mediated by N-type calcium channels in CA1. *J Neurophysiol* 105(3):1051–1062.
42. Sigel E, et al. (2011) The major central endocannabinoid directly acts at $GABA_(A)$ receptors. *Proc Natl Acad Sci USA* 108(44):18150–18155.
43. Cortes JM, et al. (2013) Short-term synaptic plasticity in the deterministic Tsodyks-Markram model leads to unpredictable network dynamics. *Proc Natl Acad Sci USA* 110(41):16610–16615.
44. Lacroix JJ, Campos FV, Frezza L, Bezanilla F (2013) Molecular bases for the asynchronous activation of sodium and potassium channels required for nerve impulse generation. *Neuron* 79(4):651–657.
45. Ali AB, Todorova M (2010) Asynchronous release of GABA via tonic cannabinoid receptor activation at identified interneuron synapses in rat CA1. *Eur J Neurosci* 31(7): 1196–1207.
46. Lenz RA, Wagner JJ, Alger BE (1998) N- and L-type calcium channel involvement in depolarization-induced suppression of inhibition in rat hippocampal CA1 cells. *J Physiol* 512(Pt 1):61–73.
47. Ermentrout B (2002) *Simulating, Analyzing, and Animating Dynamical Systems: A Guide to XPPAUT for Researchers and Students* [Society for Industrial and Applied Mathematics (SIAM), Philadelphia].

SI Appendix for: Time-coded neurotransmitter release at excitatory and inhibitory synapses

Serafim Rodrigues[i] *, **Mathieu Desroches**[i] †, **Martin Krupa**[i] †, **Jesus M Cortes** ‡ § ¶, **Terrence J. Sejnowski** ‖ ** †† **and Afia B Ali**[i] ‡‡

*School of Computing and Mathematics, University of Plymouth, Plymouth PL4 8AA, UK,†Inria Sophia Antipolis Méditerranée Research Centre, MathNeuro Team, 06902 Sophia Antipolis cedex, France,‡Biocruces Health Research Institute, Cruces University Hospital, 48903, Barakaldo, Bizkaia, Spain,§Departamento de Biologia Celular e Histologia, University of the Basque Country, 48940 Leioa, Bizkaia, Spain,¶Ikerbasque: The Basque Foundation for Science. Bilbao, Spain,‖The Computational Neurobiology Laboratory,**Howard Hughes Medical Institute, Salk Institute, La Jolla, CA 92037, USA,††Division of Biological Science, University of California, San Diego, La Jolla, CA 92093, USA, and ‡‡UCL School of Pharmacy, Department of Pharmacology, University College London, London WC1N 1AX, UK.

Submitted to Proceedings of the National Academy of Sciences of the United States of America

SI-1: Derivation of the SNARE-SM model

The main elements of the proposed mathematical model are provided here. Our mathematical formulation should be regarded as a starting point for future developments and therefore is open to reinterpretation and debate. To facilitate discussion we first outline the biological model that is used to derive the mathematical model.

Biological SNARE-SM model. We closely follow the canonical model of exocytosis proposed by Thomas Südhof and Josep Rizo [48,49]. According to this model, the exocytotic core machinery is formed by SNARE proteins (SNAP-25, synaptobrevin, syntaxin-1) that possess SNARE motifs, which bind and form a four-helix bundle (containing two SNARE motifs from SNAP-25, one from synaptobrevin and one from syntaxin-1). The SNARE protein is also bound to SM (Munc18) protein therefore forming the so-called SNARE-SM complex. This core is continuously assembled and dissociated, with extensive protein folding/unfolding reactions occurring during the exocytotic/endocytotic cycle. The cycle involves a series of steps that include tethering and docking of synaptic vesicles at specialized sites called active zones, one or more priming steps that render the vesicles ready for exocytosis and fusion of vesicles with plasma membranes that is acutely triggered by Ca^{2+} entry. These steps are controlled by numerous regulatory proteins but the fundamental ones are the RIMs, Rab3/27, Munc13-1 and calcium sensors such as Synaptotagmin-1 or Synaptotagmin-7. In addition, two chaperone systems (CSP_α/Hsc70/SGT complex and α-synuclein) facilitate the maintenance of proper SNARE states. The CSP_α/Hsc70/SGT complex binds to SNAP-25 and retains it an active state capable of entering into SNARE complexes, whereas α-synuclein binds to Synatobrevin/VAMP and accelerates its ability to assemble with SNAP-25 and syntaxin-1 into SNARE complexes. In summary, the main steps are as follows (to be accompanied by Fig.S1-a):

Step 0. At the basic level, what initiates the tethering/docking of vesicles and how the active zone is generated (i.e., what proteins nucleate its assembly), is still unknown. However, RIMs are considered critical for tethering/docking by interaction with Rab3/27, for recruiting Ca^{2+} channels to the active zones and to activate vesicle priming by interaction with Munc13 [50,51]. Specifically, the N-terminal Zinc (Zn^{2+}) finger (ZF) domain of RIMs, which is flanked by α sequences (i.e. α-RIM), binds to Rab3 (via α-helical sequences) as vesicle GTP-binding proteins and also binds to Munc13 as a priming factor. In particular, Munc13-1 N-terminal C_2A domain forms a stable homodimer, which inhibits priming. The interaction of this domain with N-terminal Zinc (Zn^{2+}) finger (ZF) domain of α-RIMs enables Munc13-1/α-RIM heterodimerization, thus triggering priming. The whole interaction is called the tripartite complex Munc13/RIM/Rab3 formation that functions as a switch between docking and vesicle priming (Stage I) [52].

Transition from Step 0 to Step 1. Munc13 mediates/gates transition from closed-Syntaxin/Munc18 complex to the SNARE complex formation. Specifically, in the initial conformation of Syntaxin-1, its N-terminal H_{abc} domain folds back on its SNARE motif, thus forming a "closed" state. It also binds to Munc18-1. Essentially, Munc18-1 stabilizes the closed-conformation of Syntaxin-1 and acts as a negative regulator preventing Syntaxin-1 from assembling into the SNARE complex (i.e. preventing fusion by blocking SNARE complex assembly). Subsequently, the MUN domain of Munc13 weakly interacts with the SNARE motif of Syntaxin-1, enabling it to have a transition to an "open" conformation gating the way to Step 1.

Step 1. Syntaxin-1 SNARE motif becomes available for binding with SNAP-25 and Synaptobrevin. In addition, Munc18-1 translocates to also bind with the SNAREs (i.e. the Munc13-MUN/SNARE complex/Munc18-1 macromolecule is formed) [53]. Thus, before the fusion signal arrives, a reversible or partially assembled Trans-SNARE complex is formed (i.e. Half-zipped four-helical bundle of SNARE complex), which exists in a dynamic equilibrium between loose and tight form [54].

Transition from Step 1 to Step 2. Complexin and synaptotagmin (a calcium sensor) are two functionally interdependent key proteins, where complexin is a co-factor that functions both as a clamp and as an activator of calcium-triggered fusion. Complexin initiates the second priming stage that prepares the SNARE-SM complex for fusion by binding to partial trans-SNARE complex and stabilizing the interactions between the SNARE motifs of synaptobrevin and syntaxin. Sub-

[i] Authors with equal contribution

Reserved for Publication Footnotes

sequently, calcium-activated synaptotagmin competes with complexin for SNARE complex binding (by displacing part of complexin), thereby triggering pore opening. Specifically, synaptotagmin contains two-calcium binding domains (C_2A and C_2B). Experiments suggest that calcium binds to C_2B in order to regulate the precise timing required for coupling vesicle fusion to calcium influx. Then Ca^{2+}-dependent interactions between C_2A domain and membranes generate an electrostatic switch that initiates fusion [55]. However, it must be noted that the precise binding mode of synaptotagmin with SNARE complex, as well as fusion pore opening mechanism, is still being debated [48, 56].

Step 3. Membrane fusion in itself is a complex phenomenon involving chemical, mechanical and electrostatic forces that are nonlinear (e.g. hysteresis phenomena) as well as phospholipids bilayers, which undergo a phase transition between ordered (gel) and disordered (liquid-crystalline) liquid states. Assembly of the full trans-SNARE complex (together with the SM proteins) brings the vesicle and plasma membranes to within 4 nm and opens the fusion pore. This involves removal of hydration layers, local membrane bending that forms protuberances called nipples, merging of the two proximal leaflets generating a so-called stalk intermediate, and formation of a fusion pore. The fusion pore expansion transforms the initial trans-SNARE into cis-SNARE complex [48].

Step 4. After fusion, core-complexes that remain on the same membrane (cis-core complexes) are disassembled (by ATP hydrolysis via NSF binding to the core-complex through SNAPs), thus completing the cycle.

Mathematical derivation of the SNARE-SM model
The complexity of the aforementioned protein/protein interactions involves complex biophysical processes such as heterogeneous catalysis (e.g. calcium binding to C_2A domains via the Langmuir-Hinshelwood mechanism), allosteric regulations and phase transitions of phospholipid bilayers, among others. A well-defined mathematical framework for protein-protein interactions is still wanting [57,58]. However, approximations based on mass-action laws have been used to model protein interactions [59], which we have adopted here. To derive the model's equation, we separated the initiation of the exocytotic cycle (*Step 0*) from the cycle itself (*Steps 1–4*). Specifically, for the exocytotic cycle, we followed the approach proposed by Tyson in [59] and we extend it by using principles of multi-timescale dynamical systems theory [60,61]. The exocytosis trigger (*Step 0*) is modeled by a nonlinear switch which can be seen as the crossing of an energy barrier.
Following Fig.S1-b, which describes the schematic diagram showing the set of kinetic protein reactions involved in the exocytotic cycle, we obtain the following differential equations:

$$\frac{d[SM'-S]}{dt} = k_4[TSS] - k_1[SM'-S], \quad [\mathbf{1}]$$

$$\frac{d[PSS]}{dt} = k_1[SM'-S] - [PSS]\,\mathbf{F}\Big([TSS]\Big), \quad [\mathbf{2}]$$

$$\frac{d[TSS]}{dt} = [PSS]\,\mathbf{F}\Big([TSS]\Big) - k_4[TSS], \quad [\mathbf{3}]$$

where $[SM'-S]$ represents a complex formed by Munc18 and Syntaxin-1 in its "open" conformation, $[PSS]$ represents a Partial SNARE complex and $[TSS]$ a Trans/Cis SNARE complex. The constants represent the interaction rates between the SNARE-SM proteins and the action of regulatory proteins (relate these to the circled numbers in Fig.S1-b). More precisely,

- k_1 is related to the action of Complexin, SNAP25, VAMP2 and chaperones CSP_α/Hsc70/SGT complex and α-synuclein;
- k_2 is related to the action of Synaptotagmin;
- k_3 is related to the action of ATP, NSF and SNAP;
- k_4 is related to ADP+NSF+SNAP, which dissociate the SNARE and the SM proteins.

The function $\mathbf{F}$ embeds the complexity of fusion pore formation and fusion pore expansion that transforms the initial Trans-SNARE into Cis-SNARE complex. This highly nonlinear process can be seen as an autocatalysis (if one remains within the viewpoint of mass-action laws) because Trans-SNARE and Cis-SNARE are the same proteins but undergoing auto-reaction enabling pore expansion. Alternatively, because this process involves electrostatic and mechanical forces, we can model it phenomenologically. We minimally describe this complex process using a nonlinear quadratic function. Note that $\mathbf{F}$ includes the rate constants k_2 and k_3.
We now define our macroscopic variables p_1 and p_2 by

$$p_1 = [\mathsf{PSS}]+[\mathsf{TSS}],$$
$$p_2 = [\mathsf{TSS}].$$

This can be viewed as a dichotomy between the interactions taking place prior to fusion (represented by p_1) and during/after fusion (represented by p_2). Furthermore, the macromolecule represented by variable $[SM'\text{-}S]$ (i.e. Synatxin-1/Munc18) is constantly attached all through the exocytosis cycle as predicted by Thomas Südhof's and Josep Rizo's model [48,49]. Thus it is a key molecule to which all other proteins will attach during exocytosis. Therefore, we assume that this quantity is preserved and, hence, remains constant during the cycle. Consequently, we obtain from equations [**2**] and [**3**]

$$\frac{dp_1}{dt} = \widehat{k_1} - k_4 p_2, \quad [\mathbf{4}]$$

$$\frac{dp_2}{dt} = (p_1 - p_2)\mathbf{F}(p_2) - k_4 p_2, \quad [\mathbf{5}]$$

where $\widehat{k_1} = k_1[SM'-S]$ and we assume F to have no constant term (which can be justified by the presence of a 'dynamic equilibrium' as explained in *Step 1*). Hence, we can rewrite the term $(p_1-p_2)\mathbf{F}(p2)$ in equation [**5**] as $p_2\widehat{\mathbf{F}}(p_1,p_2)$, where the function $\widehat{\mathbf{F}}$ is quadratic in p_2 and has its zero level-set (i.e. the set $\{\widehat{\mathbf{F}} = 0\}$) crossing transversally the horizontal axis $\{p_2 = 0\}$. This axis represents the 'dynamic equilibrium' as will become clear in subsequent Sections. The crossing point corresponds to our "transcritical point' (see interaction **Slow-fast decomposition** below). The above manipulations allow us to recast system [**4**]–[**5**] as

$$\frac{dp_1}{dt} = \varepsilon(\alpha - p_2), \quad [\mathbf{6}]$$

$$\frac{dp_2}{dt} = p_2\Big(\widehat{\mathbf{F}}(p_1,p_2) - k_4\Big). \quad [\mathbf{7}]$$

Here we assume that $\widehat{k_1}$ and k_4 are small, both proportional to a small parameter $0 < \varepsilon \ll 1$. These are reasonable assumptions for the following reasons: Parameter $\widehat{k_1}$ can be related to the clamping action of complexin, which delays neurotransmitter release (see *Step 1*); parameter k_4 can be related to the dissociation of the involved proteins and subsequent endocytosis, which is typically slower than exocytosis (see *Step 4*); The small parameter ε induces a timescale separation into the model, making p_1 a slow variable and p_2 a fast variable. Note that equations [**6**]–[**7**] can be seen as a

perturbation of the model obtained by Tyson in [59]. Interestingly, our derived equations ([**6**]–[**7**]) have the same form as the Rosenzweig/MacArthur model [62], which expresses delayed activity between macroscopic variables via a "dynamic transcritical bifurcation". (See Section SI-2 below for more details.)

We now consider modeling the *Transition from Step 0 to Step 1*. In order to keep the model parsimonious, the initiation of priming (Stage I) by the reversal of the auto-inhibition of Munc13 and subsequent transition to SNARE-SM complex formation is modeled directly with variables p_1 and p_2. This is clearly a nonlinear switch, so we choose to model it via a quadratic nonlinearity in both p_1 and p_2. The chosen degree of this nonlinear function can be related to the fact that this activation process involves the crossing of an energy barrier. Therefore, the nonlinear function that we use to model this transition has the form

$$G(p_1,p_2)=\Big(p_2-(ap_1+b)\Big)\Big(p_2-(\tilde{a}p_1+\tilde{b})\Big).$$

Parameters a, b, $\tilde{a}$ and $\tilde{b}$ control the activation of the nonlinear switch; this will become clear in paragraph "SNARE-SM model phase-space". The geometry induced by the function G, to be placed in equation [**6**], will be explained in Section SI-2 below.

The full SNARE-SM model. Following the above derivation, we are now in position to introduce the full SNARE-SM model, whose equation have the form:

$$p_1{}' = \varepsilon G(p_1,p_2)\big(\alpha-p_2\big)+V_{in}(t) \qquad [\mathbf{8}]$$

$$p_2{}' = p_2\Big(p_1-\big(\kappa_2p_2^2+\kappa_1p_2+\kappa_0\big)\Big), \qquad [\mathbf{9}]$$

where the primes represent time derivatives ($\frac{d}{dt}$) and, at a macroscopic scale, $V_{in}(t)$ corresponds to a pre-synaptic stimulus (e.g. calcium influx). Note that G enters equation [**8**] as a perturbation, therefore activating both p_1 and p_2 upon the arrival of an incoming pre-synaptic stimulus. Furthermore, the input $V_{in}(t)$ is what allows to activate the nonlinear switch represented by the function G; this will be explained in Section SI-2. Now, comparing equation [**9**] with equation [**7**], we can immediately see that $\kappa_0=k_4$ and that $\widehat{F}(p_1,p_2)=p_1-\big(\kappa_2p_2^2+\kappa_1p_2\big)$, where the parameters κ_1 and κ_2 can be non-trivially related to the rate constants k_2 and k_3, hence gives them clear biophysical interpretations. The resulting model exhibits features of slow, evoked irregular and spontaneous activations. The mathematical novelty of the proposed model is that it combines *dynamic transcritical bifurcation* with an *excitable structure* that depends on an input signal. This gives rise to a new mathematical structure, which we call an *activity induced-transcritical canard* that can generate delayed and irregular responses to an input. The dynamic repertoire of the model therefore includes *excitability*, *delayed responses to input stimuli* and *limit-cycle dynamics*. From a biological view point, this unifying framework explains otherwise isolated features of differential exocytosis based on known mechanisms.

SI-2: SNARE-SM Model dynamics

Equations [**8**]–[**9**] determine the three modes of neurotransmitter release, which mathematically translates to the SNARE-SM model's mode *excitability*, *delayed response to input stimuli* or *limit-cycle dynamics*. Setting the right-hand side of system [**8**]–[**9**] to zero gives the equations for its *nullclines* which, when plotted in the two-dimensional space (*phase-space*) reveal the three equilibria of the system. Namely, a *stable equilibrium* S, an *unstable equilibrium of saddle type* U, and an unstable equilibrium $\widetilde{\mathsf{U}}$, as mapped out in Fig.S1-c. Two other points lie on the nullclines and are important for the global dynamics of the model; they are labeled SN (*saddle-node* transition point) and TC (*transcritical* transition point) (Fig.S1-c), which generate all the functions associated with each stage of the exocytosis-endocytosis cycle. The transcritical point can perturb, upon variation some model parameters, to two points of SN type, which then gives the geometry of Tyson's model; see Fig.S1-d.

SNARE-SM model phase-space. The fast nullcline, defined by $p_2{}'=0$, is formed by two connected components, one component being the horizontal line $\Gamma_1\equiv\{p_2=0\}$ (can be related to a reversible or partially assembled Trans-SNARE complex which exists in a dynamic equilibrium between loose and tight form) and the second being the parabola $\Gamma_2\equiv\{\kappa_2p_2^2+\kappa_1p_2+\kappa_0\}$. The pale blue shaded rectangle in Fig.S1-c indicates the region of negative values of p_2, which from a biological point of view is irrelevant and thus will not be considered for the model dynamics. The solid half-line and half-parabola indicate regions of stable quasi-stationary activity, while the dashed ones indicate regions of unstable quasi-stationary activity. The SN (*saddle-node equilibrium bifurcation*) is a special transition point that separates the quasi-stationary stable from the quasi-stationary unstable activities on the parabola Γ_2. A similar point exists on the line Γ_1, this is the transition point TC.

Slow-fast decomposition. Both transition points SN and TC are well-defined in the limit $\varepsilon=0$ of the SNARE-SM model, which yields the so-called *fast subsystem* of [**8**]–[**9**]. Given that the parameter ε is taken to be positive and small, this limit is very natural to consider as an approximation to the fast dynamics of the full system. Indeed, in the fast subsystem, only p_2 still evolves dynamically while p_1 functions as a parameter ($p_1{}'=0$). The resulting one-dimensional system has equilibria, which depend on value of p_1 as a parameter. This dependence is encoded into the p_2-nullcline, which then corresponds to families of equilibria of the fast subsystem. These equilibria may undergo bifurcations as p_1 is (statically) varied. In particular, the emerging bifurcations are saddle-node bifurcations (this is the meaning of the transition point SN) or transcritical bifurcation (this is the meaning of the transition point TC).

Transition points are therefore bifurcation points of the fast subsystem, however, they are not bifurcation points of the full system. Nonetheless, they influence the global dynamics of system [**8**]–[**9**] by inducing switches between two different levels of quasi-stationary activity, one close to Γ_1 and the other close to Γ_2; they are termed *dynamics bifurcations* for the full system. Therefore, families of equilibria of the fast subsystem translate into loci of quasi-stationary activity of the full system, this activity switching from the vicinity of Γ_1 to that of Γ_2 near both SN and TC. The behaviour near TC is structurally different from that near SN and induces a delay to the switching. This is the core phenomenon behind the SNARE-SM model.

The three equilibria of system [**8**]–[**9**], S (*stable*), U (*unstable of saddle type*) and $\widetilde{\mathsf{U}}$ (*unstable*) correspond to three (coexisting) equilibrium solutions of the system, for a given set of parameter values. Note, the condition $b\leq\tilde{b}$ is the only case considered herein, since this renders S stable and U unstable. Also, the condition ($\alpha<-\kappa_1/(2\kappa_2)$) is used, which makes $\widetilde{\mathsf{U}}$ unstable and does not affect the overall dynamics of the system. However, when α is close to the p_2-coordinate of

the SN point then special limiting cases emerge (see section **SNARE-SM model exceptional cases**). Π_3 divides the space into two regions, which dictates how p_1 evolves. Specifically, below Π_3 the complex p_1 evolves towards the right (i.e. its activity increases), except in the region in-between S and U, where the basin of attraction of S forces it towards inactivity. In contrast, above Π_3 the activity of p_1 decreases (see the black arrows on Γ_1 and Γ_2). The vertical line F (brown) and its corresponding arrows indicate the direction in which the fast complex p_2 evolves. This is applicable everywhere except in the outer region of the dashed parabola segment, where p_2 evolves towards Γ_1. The fast nullclines Γ_1 and Γ_2 intersect at the dynamic transcritical bifurcation point TC (with coordinates $(\kappa_0, 0)$), which characterises the exchange of stability seen simultaneously in Γ_1 and Γ_2 (transition from dashed to black lines).

As bifurcation points of the fast subsystem, SN and TC affect the full system, so to speak, as "ghost" configurations in the full system [**8**]–[**9**], when the protein complexes interact. In particular, as the trajectory of the full system flows along Γ_1 towards increasing activity of p_1, it actually does not pass directly through the TC point. Rather it flows in the vicinity of TC (within an ε vertical distance from TC); denote this coordinate passage point $(p_{1,T}, 0)$ as illustrated in Fig.S2-c (bottleneck-shaped zoom of the grey shaded rectangle of Fig.S2-a). This bottleneck structure emerges because of the interplay between contraction and expansion of the flow near the invariant line Γ_1, which changes stability at TC. It represents the way-in way-out function, which allows to determine the delay given an entry point to the left of TC.

In summary, these interactions between protein complexes (p_1, p_2) generate special transition points that induce dynamic bifurcations and regulate all the functions associated with each stage of the exocytosis-endocytosis cycle.

SNARE-SM model evoked release mode. This section examines evoked release (synchronous and asynchronous modes) in terms of both phase-diagrams and time-series (Fig.S2 and Fig.S3), which complements the biological-view point in Fig.3 (main manuscript). We recall that synchronous release initiates within [0-5) ms after an action potential while asynchronous release manifests itself only under certain conditions and sets in with a longer delay (i.e. [5-15ms) after an incoming action potential.

For evoked release mode, system [**8**]–[**9**] is set to an *excitable regime*, which corresponds to choosing b to be close to the value $(\kappa_1^2/(4\kappa_2) - \kappa_0)$. This has the effect of positioning the points S and SN vertically close to each other, SN being (vertically) to the left of S. Thus, in absence of further input spikes or of any noise, the system goes back to rest after its transient response to a stimulus. A sufficiently large amplitude of $V_{in}(t)$, or a sequence of input spikes, enables the system to escape the basin of attraction of the stable state S and go past the unstable point U. The system's activity flows along Γ_1 (specifically, an ε vertical distance away) towards increasing p_1, and past the $(p_{1,T}, 0)$ point as illustrated in Fig.S2-c (zoom of the grey shaded rectangle of Fig.S2-a). Slow-fast theory of *dynamic transcritical bifurcations* ensures that the system's activity will flow in the vicinity of Γ_1, which past the TC point is repelling/unstable in the normal direction towards the upper segment of Γ_2. However, inertia will keep the activity along Γ_1. The associated trajectories are examples of *canards orbits*. Specifically, *canards* are trajectories that contain segments following both attracting and repelling slow manifolds (in this case corresponding respectively to the half-left and half-right lines of Γ_1). Thus, the slow processes (seen as slowly-varying parameters) entrain the fast processes inducing delays and variabilities, which leads to sensitivity to initial conditions.

This phenomenon is well known in the mathematical theory of slow-fast dynamical systems and is also observed experimentally (e.g. [63]). As the inertia slowly vanishes, a sudden jump of the trajectory occurs towards the upper branch of Γ_2. However, as the flow traverses Π_3 it triggers the deactivation of p_1. The arrival of the flow onto Γ_2 also triggers the deactivation of p_2. Consequently, both p_1 and p_2 down regulate their activity, passing via the SN point and finally become inactive (S). The delayed response of the system to an input is entirely governed by the nullclines of the fast system and by the so-called *way-in-way-out function* (see next section), which measures the balance between the contraction rate (attraction or binding) towards Γ_1 (to the left of TC) and subsequent expansion rate (repelling or un-binding) away from Γ_1 (towards the right of TC). Therefore, this allows full control of the delay by suitably tuning system parameters, in particular ε, as well as initial conditions. Consequently, synchronous and asynchronous response regimes result from a minor parameter change (see Table S1, 2nd-3rd columns).

Following Fig.S2 we note that a change in initial conditions shows variability in the delayed response, which in this case varies between 8 to 12 time units; compare the magenta, red and cyan responses in panel (b2) for the same input signal from panel (b1). The synchronous mode is shown in Fig.S3-a-a1-a2 (phase-diagram and time-series). Here, the time scale separation between the protein complexes is reduced, which induce output responses occurring within one time unit. Panels b-b1-b2 and c-c1-c2 of Fig.S3 demonstrate that the model can support delayed and irregular activations upon different stimulus (i.e. in terms of number of inputs and frequency).

SNARE-SM model spontaneous release mode. This section examines the two modes of spontaneous release in terms of phase diagrams. Similarly to the evoked release mode, the first form of spontaneous release is set by placing the system into an *excitable regime*, see Table S1 (4th column). However, the distance between S and U points is small enough so that a small noise perturbation is sufficient to trigger an exocytotic-endocytotic cycle; compare phase-diagram in Fig.S4-a and time-series in Fig.S4-a1. In particular, a noise term is added in the p_1-direction enabling the activity to escape the basin of attraction of the stable state S thus leading to an exocytotic-endocytotic cycle.

The alternative spontaneous release mode is set by placing the system in a *limit-cycle* regime, see Table S1 (5th column). The self-sustained oscillation is triggered by moving S and U to the left (along Γ_1) so that none of them is vertically aligned with the SN point. This is illustrated by phase-diagram Fig.S4-b, which complements the time series of Fig.S4-b1. The oscillations can be made irregular by modulating the position of Γ_2, for instance, by perturbing it with noise. Note that in both forms of spontaneous activations, the width of Γ_2 is made small in order to relate to the *kiss-and-run* endocytosis that mediates release of neurotransmitters in small quantities.
Note that for all release modes, we have chosen to show in panels ai,bi,ci (i=1,2,3) of Fig.S2 to Fig.S5, the time traces of the SNARE-SM model with dimensionless time (t).

SNARE-SM model's way-in-way-out function. A delay induced by a dynamic bifurcation can be estimated by the so-called entry/exit or *way-in-way-out function*; see [52] for details. For completeness, a brief description of its formulation is provided. As discussed, the SNARE-SM model, system [**8**]–

[**9**], possesses a family of quasi-stationary points along Γ_1 with a dynamic transcritical bifurcation TC at $(p_{1,T}, 0)$ where $p_{1,T} = \kappa_0$ (see Fig.S2-c, shaded region). Thus every initial condition $(p_{1,0}, p_{2,0})$, taken in the vicinity of Γ_1 with $p_{1,0} < p_{1,T}$ results in a trajectory that is quickly attracted to an ε-neighbourhood of Γ_1 and towards increasing p_1 activity. The trajectory flow passes through $p_{1,T}$ and continues to follow the (now repelling) horizontal axis until it gets repelled in exit point $p_{1,ex}$. The exit point is determined as a function of the entry point. This functional relationship can be established equivalently in terms of exit and entry times, since along Γ_1 the slow variable p_1 is a simple drift and thus behaves like time. Given a system in the following general form (satisfied by the SNARE-SM model [**8**]–[**9**]),

$$\begin{aligned} \dot{p_1} &= H(p_1, p_2) \\ \varepsilon \dot{p_2} &= W(p_1, p_2), \end{aligned} \qquad [\mathbf{10}]$$

then the exit time t_{ex} is defined uniquely via the following entry/exit condition

$$\int_0^{t_{ex}} W_{p_2}(p(t))dt = 0. \qquad [\mathbf{11}]$$

Here the overdot denotes derivation with respect to another time parametrisation, namely, $\tau = t/\varepsilon$; systems [**8**]–[**9**] and [**10**] are equivalent as long as $\varepsilon \neq 0$, the limits $\varepsilon = 0$ being diferent (approximation of the fast dynamics in the case of [**8**]–[**9**], and of the slow dynamics in [**10**]). The function W_{p_2} is the derivative of W with respect to p_2 and $p(t) = (p_1(t), 0)$, where $p_1(t)$ is the solution of the slow system $\dot{p_1} = H(p_1, 0)$ with initial condition $p_{1,0}$. For the SNARE-SM model, the slow subsystem is, $\dot{p_1} = \alpha(ap + b)(\tilde{a}p + \tilde{b}) \equiv R_2p^2 + R_1p + R_0$, which corresponds to a Riccati equation with constant coefficients, therefore a separable equation that can be explicitly solved for any triple (R_0, R_1, R_2) using the equality

$$\int \frac{dp_1}{R_2p_1^2 + R_1p_1 + R_0} \quad = \quad \int dt. \qquad [\mathbf{12}]$$

Consequently, assuming only the presence of the transcritical bifurcation point, the entry/exit formula is explicit for the SNARE-SM model. However, in the SNARE-SM model the dynamics resulting from the presence of the unstable point U introduces a small bias in the estimation of the delay and the exact exit point. This estimation error is not critical for the present study. The precise estimation is beyond the scope of the present work and will be matter of future considerations since the complete *way-in-way-out function* will encode all the information about delayed release.

SNARE-SM model exceptional cases. Exceptional solutions of the SNARE-SM model are subsequently discussed. These limit case solutions are very sensitive to perturbations, so that numerical integration may be insufficient to compute them; moreover, some of them are unstable. A reliable method to compute them is the so-called *pseudo-arclength numerical continuation methods* provided by, e.g., the software package XPPAUT. From a biological viewpoint these are extremely rare events, nevertheless, for completeness they are herein described. The exceptional regimes correspond to having the slow nullcline Π_3 intersect Γ_2 at an order-ε distance from the fold point (SN); see Fig.S1-c. Specifically, α must be ε-close to the value $-\kappa_1/(2\kappa_2)$ and it can only vary by an exponentially small quantity (in ε), showing that these solutions are not persistent. Nonetheless, this induces the so-called *fold-initiated canard cycles* [64], which correspond to trajectories that do not immediately drop off the fold point, SN, but rather follow for some time the lower repelling branch of Γ_2. There exists a whole family of such canard cycles parameterized in this case by α.

Three particular cases of such cycles are shown in Fig.S5 panels a-a1-a2-a3 (compare the phase-diagrams and time series); these were computed using numerical continuation with the software package AUTO [65]. The canard denoted C_h (red) is an example of so-called *headless canard* [64], where the trajectory flows along the repelling branch of Γ_2 and then jumps back to the attracting branch of Γ_2 (upper part of the parabola). In other words, C_h oscillates around the fold point SN and may represent vesicles escaping pathologically the release cycle; see panels (a) and (b1). The largest headless canard is called *maximal canard*, C_m [64]. This corresponds to a canard cycle following the repelling branch Γ_2 for the longest segment, that is, down to the transcritical point TC; see panels (a) and (b2). The remaining canard, denoted C_{wh}, as shown in panels (a) and (b3), is an example of so called *canard with head* [64]. Such a canard cycle owes its name to the fact that, in contrast to previous cases, it follows the repelling branch of Γ_2 and instead jumps towards Γ_1, giving rise to a cycle that changes its curvature. In this case, following the jump the trajectory passes ε-close to the transcritical point TC (more specifically $p_{1,T}$; see Fig.S2-c) and, hence, enters a delayed release cycle.

The canard cycle is a stable *limit cycle* that repeats indefinitely, and this could represent yet another form of spontaneous release but one in which at least one spike stimulus is required to initiate the process. The point in the vicinity of Γ_1 (an ε vertical-distance away) onto which the trajectory lands after leaving the repelling branch of Γ_2 determines the entry point of the *way-in-way-out function* and thus determines the duration of the delay. The closer this entry point is to the unstable point U, the longer the delay will be. In the limit, where the entry point aligns vertically with the U point, the trajectory will flow along the *stable manifold* of U (typically denoted as $W^s(\mathsf{U})$) and will take an infinite amount of time to converge to U. The critical value of α that leads to this scenario marks the mathematical boundary between periodic and non-periodic regimes. In particular, this critical α marks the termination of canard cycles but also the initiation of solutions that emerge from U and flow along Γ_1 towards increasing values of p_1 (i.e. the *unstable manifold* of U, typically denoted as $W^u(\mathsf{U})$).

The family of canard cycles terminates in a connection at infinity between the stable and unstable manifolds of U, that is, a *homoclinic bifurcation at infinity*. Beyond that critical value of α, the canard trajectories follow the repelling branch of Γ_2 past the SN point, jump and land in the vicinity (an ε vertical-distance away) of Γ_1 to the left of U, which results in a flow towards the stable equilibrium point S. A further exceptional case worth noting is that, since Γ_1 is an invariant manifold (line) even for $\varepsilon > 0$, then an initial condition exactly on Γ_1 leads to a trajectory that stays on it for all future times, hence resulting in an unbounded delay. However, this case corresponds to a pathological scenario where the protein p_2 is 0 (i.e. vanishes). Finally, it is worth remarking that all the above cases are not robust to noise and thus are not representative of a typical exocytosis-endocytosis cycle.

E-SNARE-SM model, simulations and data-fitting. The SNARE-SM model feeds its output signal, p_2, into the Markram-Tsodyks' (MT) model [66,67,68] as well as into the equations modelling post-synaptic induced currents responsible for the activation of post-synaptic potentials (PSP). Consequently the E-SNARE-SM model is composed by sys-

tem [8]–[9] and the following set of equations:

$$\dot{d} = (1-d)/\tau_D - df p_2 \quad [13]$$

$$\dot{f} = (f_0 - f)/\tau_F + F(1-f)p_2, \quad [14]$$

representing the MT equations, and the dynamics of PSP, described by the following conductance-based equations:

$$\dot{g}_{\text{syn}} = -g_{\text{syn}}/\tau_{\text{syn}} + \overline{g}_{\text{syn}} df p_2 \quad [15]$$

$$C\dot{v} = -g_L(v - E_L) - g_{\text{syn}}(v - E_{\text{syn}}). \quad [16]$$

The MT-model (13)-(14) is sometimes termed the *vesicle depletion model* as it describes the time evolution of finite resources (e.g. a vesicle pool). The synaptic resources (in the pre-synaptic terminal) can be in two states: *available* to be released or *non-available* for release. The overall fraction of available vesicles is $d(t)$ and the non-available vesicles is $1 - d(t)$. The activation of the exocytotic machinery mediated by the SNARE-SM model outputs signal p_2, which feeds into the MT-model, leading to consumption of resources. The consumption rate in the transition from $d(t)$ to $1-d(t)$ is proportional to $p_2(t)f(t)$, which leads to depression. The recovery from *non-available* to *available* states occurs at a rate $1/\tau_d$, where τ_d represents the spontaneous recovery time from the depressed state. The variable $f(t)$ controls the release probability of available neurotransmitters. The transition from *non-releasable* to *releasable* has rate $Fp_2(t)$, which describes activity-induced facilitation. The reversed transition occurs spontaneously at a rate $(f_0 - f)/\tau_f$, where f_0 is the baseline activity of $f(t)$. Therefore, the amount of neurotransmitter released at a given time t is quantified as $T(t) = d(t)f(t)$.

Parameters for the MT-model were adopted from the papers by Markram and Tsodyks; however, further parameter fitting from experimental data was performed (Table S2 for inhibitory data and Table S3 for excitatory data). The output of the SNARE-SM model (p_2) also modulates the quantity of neurotransmitters released (T), which enable receptor activation and in turn causes post-synaptic potentials (PSP). In particular, the voltage equation (16), represented by the variable $v(t)$, describes PSP activations, which is induced by post-synaptic currents (PSC), $I_{\text{syn}} = g_{\text{syn}}(v - E_{\text{syn}})$, where E_{syn} is the reversal potential. Specifically, we employ GABA_A for the case of inhibitory currents and AMPA for excitatory currents. The fist term of the right-hand side of the voltage equation represents the leaky current, g_L being the leaky conductance and E_L the leaky reversal potential. Parameter C represents the membrane capacitance. The conductance, g_{syn} follows a first-order kinetic equation. Upon binding of neurotransmitters, the conductance increases by the amount $\overline{g}_{\text{syn}} df p_2$, where $\overline{g}_{\text{syn}}$ is the maximal conductance, $d(t).f(t)$ is the amount of neurotransmitter released and p_2 represents the final protein signalling process that activates the neurotransmitter release. We note that this coupling departs from the MT modelling approach, where a pre-synaptic action potential is directly used. The unbinding of neurotransmitters decreases the conductance, which occurs with a finite decay time τ_{syn}. Table S2 shows the parameter values (and their range) for parameter fitting of the E-SNARE-SM model from paired whole-cell recordings of CCK positive SCA interneurons. Table S3 shows the parameter values (and their range) for parameter fitting of the E-SNARE-SM model from paired whole-cell of the calyx-of-Held synapse.

Calibration of the model. The model is precisely captures the delay associated with every release event. In general, the dataset of a dual whole-cell recording displays n unitary IPSPs/EPSPs release events, each one having a particular delay τ_n associated to it. The delays τ_n are first measured directly from the data. Then, the most efficient way is to split the calibration procedure into n epochs, one per release event. During each epoch, the delay to release is organized by the (p_1, p_2) variables of our SNARE-SM model, and precisely controlled by the so-called "way-in-way-out" function. The output of the SNARE-SM mode is then feed-forwarded to the MT model. Therefore, the general algorithmic procedure to calibrate the full model in order to fit a synaptic dual whole-cell recording is as follows:

1. Record the way-in value $p_{1,0}$ of p_1, as p_2 crosses a predefined value $\delta \ll 1$ (which is of order ε); this corresponds to entering the pink zone in Fig.S2-a and Fig.S2-c.

2. Compute a parameter set of the (p_1, p_2) model so that the way-out value for p_1 corresponds to a transition time of τ_i; one will use the way-in value of p_1 and the knowledge of the way-in-way-out function, as well as use a classical minimisation procedure such as

$$\underset{\alpha}{\text{argmin}}(\text{dist}(\text{Model}(t;\alpha), \text{data}(t)),$$

α corresponding to the set of parameters of the model, and dist being a distance measure.

3. Record the way-out value $p_{1,ex}$ of p_1, which correspond to the moment when p_2 increases sharply, hence activating the MT model (see again Fig.S2)

4. Finally, calibrate the parameters of the MT model as done in [65].

Asynchronous release is an irregular activity not only in terms of release timing but also in terms of amplitude of the EPSP/IPSC. This means that it is much more difficult to fit associated data with the MT model, hence the epoch-fitting that we have performed. Finally, note that we have not performed an event-to-event parameter fitting given we obtained good agreement by grouping several release events together.

SI-3: Experimental data

Sampled paired whole-cell recordings obtained from unitary synapses between CCK-positive SCA interneurons in the CA1 region of P18-21 rat hippocampus are shown in Fig.S7. The data show synchronous, asynchronous, spontaneous activations as well as short-term synaptic plasticity. Also compare the single-trial experiments with the averaging over trials.

48. Rizo J., Südhof T. C. (2012) The Membrane Fusion Enigma: SNAREs, Sec1/Munc18 Proteins, and Their Accomplices - Guilty as Charged? Annual Review of Cell and Developmental Biology, 28: 279–308
49. Südhof T. C. (2014) The molecular machinery of neurotransmitter release (Nobel lecture). Angewandte Chemie International Edition 53(47): 12696–12717.
50. Deng L. et. al. (2011) RIM Proteins Activate Vesicle Priming by Reversing Autoinhibitory Homodimerization of Munc13. Neuron 69(2): 317–331.
51. Lu J. et. al. (2006) Structural Basis for a Munc13-1 Homodimer to Munc13-1/RIM Heterodimer Switch. PLoS Biol 4(7): e192.
52. Dulubova, I. et. al. (2005) A Munc13/RIM/Rab3 tripartite complex: from priming to plasticity? The EMBO journal 24(16): 2839–2850.

53. Cong M. et. al. (2011) Munc13 mediates the transition from the closed syntaxin–Munc18 complex to the SNARE complex. Nature structural & molecular biology 18(5): 542–549.
54. Tao X. et. al. (1999) Inhibition of SNARE complex assembly differentially affects kinetic components of exocytosis. Cell 99(7): 713–722.
55. Striegel A. R. e.t al. (2012) Calcium binding by synaptotagmin's C2A domain is an essential element of the electrostatic switch that triggers synchronous synaptic transmission. The Journal of Neuroscience 32(4): 1253–1260.
56. Brewer K. D. et. al. (2015) Dynamic binding mode of a Synaptotagmin-1-SNARE complex in solution. Nature structural & molecular biology 22(7): 555–564.
57. Kastritis P. L. and Bonvin A. M. J. J. (2012) On the binding affinity of macromolecular interactions: daring to ask why protein interact. J Roy Soc Interface 10(79): 20120835.
58. Howard J. (2009) Mechanical signalling in networks on motors and cytoskeletal proteins. Annu Rev Biophys 38: 217–234.
59. Tyson J. J. (1991) Modeling the cell division cycle: cdc2 and cyclin interactions. Proc Natl Acad Sci USA 88(16): 7328–7332.
60. Krupa M, Szmolyan P (2001) Extending geometric singular perturbation theory to nonhyperbolic points—fold and canard points in two dimensions. SIAM J Math Anal 33(2): 286–314.
61. Boudjellaba H, Sari T (2009) Dynamic transcritical bifurcations in a class of slow-fast predator-prey models. J Differ Equations 246(6): 2205–2225.
62. Rosenzweig ML, MacArthur RH (1963) Graphical representation and stability conditions of predator-prey interactions. Am Nat 97(895): 209–223.
63. Strizhak .P, Menzinger M. (1996) Slow passage through a supercritical Hopf bifurcation: Time-delayed response in the Belousov–Zhabotinsky reaction in a batch reactor. J Chem Phys 105(24): 10905.
64. Krupa M., Szmolyan P. (2001) Relaxation Oscillations and Canard Explosion. J Differential Equations 174(2): 312–368.
65. Doedel E. J. et al. (2007) AUTO-07p. Continuation and bifurcation software for ordinary differential equations. available at : http://http://indy.cs.concordia.ca/auto/.
66. Tsodyks M., Pawelzik K., Markram H. (1998) Neural networks with dynamic synapses. Neural computation 10(4): 821–835.
67. Hennig M. (2013) Theoretical models of synaptic short-term plasticity. Frontiers in Computational Neuroscience 7: 00045.
68. Izhikevich E. M., Desai N. S., Walcott E. C., Hoppensteadt, F. C. (2003) Bursts as a unit of neural information: selective communication via resonance. Trends in Neuroscience 26(3): 161–167.
69. Nadkarni S., Bartol T. M., Stevens C. F., Sejnowski T. J., Levine, H. (2012) Short-term plasticity constrains spatial organization of a hippocampal presynaptic terminal. Proc Natl Acad Sci USA 109(36): 14657–14662.

Caption of Table S1. Parameter values for the SNARE-SM model that allow to tune the model into the different regimes: *excitability*, *delayed responses* and *limit cycle*. The second column corresponds to synchronous release mode (excitability). The third column, asynchronous release mode (excitability and delayed response). The fourth column, spontaneous release mode via equilibria (excitability). The fifth column, spontaneous release model via limit cycle.

Caption of Table S2. Parameters for the E-SNARE-SM model. Two different values in one entry box corresponds to fitting two different epochs within a given IPSP time series.

Caption of Table S3. Parameters for the E-SNARE-SM model from paired whole-cell of the calyx-of-Held synapse. Three different values in one entry box corresponds to fitting three different epochs within a given EPSP time series.

Caption of Figure S1. Dynamics of the SNARE-SM model. a - Panel adapted from [49]. This is a Schematic representation of the biological SNARE-SM model proposed by T. Südhof and G. Rizo in [48]; the circled numbers indicate the different steps of the exocytotic cycle. b - Diagram inspired from Tyson [49] showing the kinetic protein interactions underlying the SNARE-SM model. Arrows represent transitions, the red loop represents an auto-inhibition. c -The fast nullclines $\mathsf{\Gamma}_i$, $i = 1, 2$ (corresponding to $\dot{p_2} = 0$) are shown in black. The slow nullclines $\mathsf{\Pi}_i$, $i = 1, 2, 3$ (i.e. for $\dot{p_1} = 0$) are shown in grey. A representative fast fiber F, corresponding to the fast system, where p_1 is frozen and considered as a parameter, is shown in brown. The equilibria of the SNARE-SM model correspond geometrically to intersection points between a fast nullcline and a slow nullcline. The stable equilibrium, denoted S, is marked by a black dot. The unstable equilibria, U and $\widetilde{\mathsf{U}}$, are marked by black circles. The bifurcation points of the fast system p_2 (with p_1 treated as a parameter) are indicated by stars : the saddle-node point SN and the transcritical point TC. The flow of the slow system is indicated by single black arrows on $\mathsf{\Gamma}_i$, and the flow of the fast system is indicated by double brown arrows on F. The half-plane $\{p_2 < 0\}$ (pale blue shade) emphasizes that this region is irrelevant biologically as, in cases considered here, p_2 remains strictly positive in the SNARE-SM model. d - Comparison between the SNARE-SM model and Tyson's model, which can be seen as a perturbation. The left component of $\mathsf{\Gamma}_{1-2,\mathsf{perturbed}}$ (i.e. the red cubic curve) corresponds to the fast nullcline of Tyson's model. The right component of $\mathsf{\Gamma}_{1-2,\mathsf{perturbed}}$ is unphysical because is lies in the negative p_2 half-plane.

Caption of Figure S2. Asynchronous release in the SNARE-SM model. (a) Phase diagram showing the output of the model. (b1) The input stimuli. (b2) The same information as in panel (a), but now shown in time domain. The different trajectories (cyan, red and magenta) show sensitivity to initial conditions of the delayed responses. Panel (c) zooms in the grey rectangle of panel (a) and illustrates of the *way-in-way-out function* which organizes the delay to the transcritical bifurcation $p_{1,T}$, from the entry point $p_{1,0}$ to the exit point $p_{1,ex}$. The sand-watch-like brown shaded area emphasises that trajectories are attracted towards $\mathsf{\Gamma}_1$ and after the delayed transcritical bifurcation they are repelled. For parameter values, see the third column of Table S1. Here t refers to a dimensionless time.

Caption of Figure S3. Differential release modes in the SNARE-SM model. (a-a1-a2) Synchronous release: (a) Phase diagram showing the output of the model; (a1) The input stimuli; (a2) The same information as in panel (a), but now shown in time domain. For parameter values, see the second column of Table S1. (b-b1-b2) Asynchronous release (one input spike): (b) Phase diagram showing the output of the model; (b1) The input stimuli; (b2) The same information as in panel (b), but now shown in time domain, that is, delayed release to a single input spike with arbitrary long delay. (c-c1-c2) Asynchronous release (three input spikes): (c) Phase diagram showing the output of the model; (c1) The input stimuli; (c2) The same information as in panel (c), but now shown in time domain, that is, delayed release upon a burst of input spikes. In all panels, t refers to a dimensionless time.

Caption of Figure S4. Spontaneous release in the SNARE-SM model. (a1) Spontaneous release via excitability regime shown in the phase space (model output in red). Here S and U are placed close to each other and the amplitude of $\mathsf{\Gamma}_2$ is decreased. Noise is added in the p_1-direction, which allows the flow to escape the basin of attraction of the stable equilibria S. (b1) The same information as in panel (a1), but now shown in time domain. (b1) Spontaneous release via a limit cycle regime shown in phase space (model output in red). Here S and U are placed to the left of $\mathsf{\Gamma}_1$ leading to a non vertical alignment with the SN point, which results into a limit cycle. The limit cycle is made irregular by adding small noise to $\mathsf{\Gamma}_2$. (b2) The same information as in panel (a2), but now shown in time domain. For parameter values, see the fourth and fifth columns of Table S1, respectively. Here t refers to a dimensionless time.

Caption of Figure S5. Specific dynamics of the SNARE-SM model. (a) Shows exceptional trajectories, namely *canard cycles [60,64]*, of the SNARE-SM model in phase diagram. These cycles follow the repelling branch of $\mathsf{\Gamma}_2$ (past the saddle node point SN) for an order-1 length. Three different cases are shown. First case: a *headless canard*, C_h (red) completes its cycle by following a fast segment upwards back to the attracting branch of $\mathsf{\Gamma}_2$. Second case: the largest *headless canard*, called *maximal canard*, C_m (blue), flows maximally until it reaches the transcritical TC point. Third case: a *canard with head*, C_{wh} (green) which, in contrast to the other cases, follows the repelling branch of $\mathsf{\Gamma}_2$ and then jumps towards $\mathsf{\Gamma}_1$ (i.e. changes its local curvature). (a1) Shows C_h in the time domain. (a2) Shows C_m in the time domain. (a3) Shows C_{mh} in the time domain. For parameter values, refer to the third column of Table S1 except for α, which varies and allows to display the family of canard cycles. However, the variation in α is within an exponentially small interval so that, for the chosen value of ε, the 11 first decimal places of the values of α for C_h, C_m and C_{wh} are the same: 0.50025024345. Subsequent panels show that, away from the canard regime, the SNARE-SM model mimics VAMP4-mediated delayed release: (b) Phase-diagram shows that intense stimulation (shown by a sequence of curved blue arrows) first generates a synchronous release and subsequently a delayed release. Initially, the unstable equilibrium U is placed to the left (when compared to the projection of SN onto $\mathsf{\Gamma}_1$). Also, S and U are sufficiently far apart so that only intense stimulation enables the activation of synchronous release and subsequent delayed release (in fact with the possibility of multiple delayed releases as the system is now in a limit-cycle regime). Terminating the delayed release cycle requires moving the unstable point U to the right (point marked $\mathsf{U}^\star$) to ensure that the endocytotic activity falls into the basin of the attraction of S. Moving U to the right may represent the modelling of some physiological process that terminates

the exocytotic-endocytotic cycle. (b1) The input stimuli. (b2) Depicts the same information as panel (b) but in the time domain. The parameter values for this case are the same as in the third column of Table S1 except for: $b = 0.05$, $\tilde{b} = 0.2$; for $\mathsf{U}^\star$, the value of $\tilde{b}$ is increased to 0.28. In all time-domain plots, t refers to a dimensionless time.

Caption of Figure S6. E-SNARE-SM model, Spike time dependent plasticity Delayed action potentials mediated by the E-SNARE-SM model can be used to study spike-time dependent plasticity. Delayed action potentials has previously been studied in a complex spatial-temporal model of short-term synaptic plasticity of the CA1-CA3 cells [69]. These plots demonstrate that endowing E-SNARE-SM model with excitable currents (herein Na^+ and K^+ currents) can reproduce the same phenomena. (a) A presynaptic spike at time instant t_{sp} induces an exocytotic-endocytotic signal p_2 (top panel), which then triggers a delayed action potential in the post-synaptic cell with delay τ (bottom panel). (b) Similar scenario as in panel (a), except that the parameters associated to delayed exocytosis are altered thus generating a different delay. (c) A two parameter curve in (ε, τ) where every point measures the time delay between the onset of a pre-synaptic spike and the peak of the triggered action potential. These results therefore shows that E-SNARE-SM model could be extended to study more complex forms of synaptic plasticity, for example Spike time dependent plasticity.

Caption of Figure S7. Dual whole-recordings of unitary synapses in CA1 region of rat hippocampus. Three types of unitary synaptic connections and spontaneous IPSPs are shown. Single sweep raw data are superimposed and average responses are shown in bold traces. (A) Inhibitory connection between Schaffer collateral associated (SCA) to other SCA interneurons displays, synaptic facilitation. (B) Unitary connections between lacunosum moleculare, radiatum, perforant pathway (LM-R PP) to SCA connections display a delayed onset of release and average IPSPs display a slow time courses. (C) Connections between back-projecting interneurons in stratum radiatum to lacunosum moleculare perforant path (LM PP), display brief train depression, typically observed at inhibitory synapses. Facilitating synapses in (A) and (B) involve presynaptic cells that are immunoreactive for the neuropeptide CCK, that co-localise CB1 receptors. (D) Show by whole-cell recordings, most of these inhibitory interneurons receive spontaneous IPSPs.

Parameters	Synch. mode	Asynch. mode	Spont. mode (eq.)	Spont. mode (cycle)
a	-1	-1	-1	-1
b	0.25	0.25	0.25	0.3
$\tilde{a}$	-1	-1	-1	-1
$\tilde{b}$	0.28	(0.28, 0.4)	0.5	0.35
α	0.4	0.4	(0.1, 0.2)	0.15
ε	$(10^{-4}, 10^{-2})$	(0.1, 0.5)	$(10^{-4}, 10^{-2})$	$(10^{-4}, 10^{-2})$
κ_0	0.3	0.5	0.68	0.66
κ_1	-0.2	-1	-1.8	(-2.5, -1.5)
κ_2	0.2	1	3	5

Table S1.

Symbol	Description	Fig.4-b1	Fig.4-b2	Fig.4-b3
$radius$	Patch radius of the electrode micro-pipet	0.2e-3cm		
$A = 4\pi(radius)^2$	The membrane area covered by the electrode	[-]cm^2		
C	Membrane capacitance	196e-6 μ F		
R	Leak membrane resistance	220 MΩ	260 MΩ	220 MΩ
$c_m = C/A$	Specific membrane capacitance	[-] μ F/ cm^2		
$r_m = R * A$	Specific membrane resistance	$[-]M\Omega$ cm^2		
$\tau_m = C * R$	Membrane time constant	43.1 ms		
E_L	Leak reversal potential	-55mV	-55mV	-55mV
τ_{gaba}	Decay time constant of $GABA_A$	25ms	6ms / 17ms	20ms
E_{gaba}	Reversal potential for $GABA_A$	-57mV	-60mV	-57mV / -57.5mV
$\bar{g}_{gaba}$	Peak $GABA_A$ conductance	1 mS/cm^2	1 mS/m^2	1mS/m^2
τ_F	Recovery time of synaptic facilitation	150 ms	1500ms / 0.15ms	2500ms
τ_D	Recovery time of synaptic depression	0.2 ms	100ms	100ms
F	Resting release probability	0.001	1 / 0.0035	0.25 / 0.7

Table S2.

Symbol	Description	Fig.5-b1	Fig.5-b2
$radius$	Patch radius of the electrode micro-pipet	0.2e-3cm	
$A = 4\pi(radius)^2$	The membrane area covered by the electrode	[-]cm^2	
C	Membrane capacitance	800e-6 μ F	
R	Leak membrane resistance	220 MΩ	
$c_m = C/A$	Specific membrane capacitance	[-] μ F/ cm^2	
$r_m = R * A$	Specific membrane resistance	$[-]M\Omega$ cm^2	
$\tau_m = C * R$	Membrane time constant	176.0 ms	
E_L	Leak reversal potential	-55mV	
τ_{ampa}	Decay time constant of $AMPA$	2.5ms	2.5ms / 7ms / 1ms
E_{ampa}	Reversal potential for $AMPA$	3mV	
$\bar{g}_{ampa}$	Peak $AMPA$ conductance	2.5 mS/cm^2	13 mS/cm^2
τ_F	Recovery time of synaptic facilitation	0.1 ms	0.1 ms / 1000 ms / 2000 ms
τ_D	Recovery time of synaptic depression	1000 ms	1000 ms / 1 ms / 0.01 ms
F	Resting release probability	1	

Table S3.

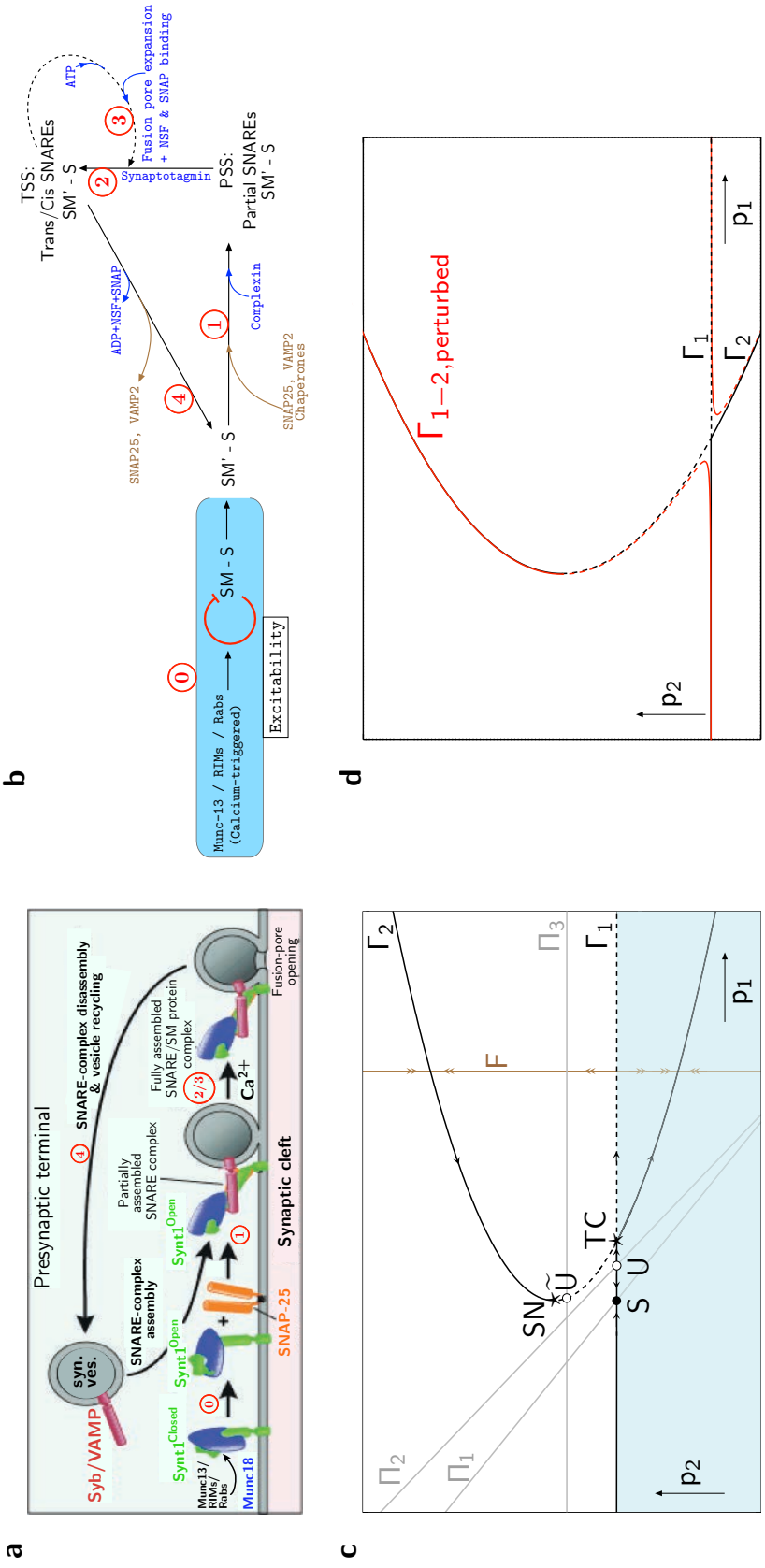
a
Presynaptic terminal
Syb/VAMP
syn. ves.
Munc18
Munc13/ RIMs/ Rabs
Synt1Closed
Synt1Open
SNARE-complex assembly
SNARE-complex disassembly & vesicle recycling
Partially assembled SNARE complex
Fully assembled SNARE/SM protein complex
Ca2+
SNAP-25
Synaptic cleft
Fusion-pore opening
b
TSS: Trans/Cis SNAREs SM' - S
PSS: Partial SNAREs SM' - S
ATP
Fusion pore expansion + NSF & SNAP binding
Synaptotagmin
ADP+NSF+SNAP
SNAP25, VAMP2
Complexin
SNAP25, VAMP2 Chaperones
Munc-13 / RIMs / Rabs (Calcium-triggered)
SM - S
Excitability
c
Γ2
Π3
Γ1
F
SN
TC
S U
Π2
Π1
p1
p2
d
Γ1−2,perturbed
Γ1
Γ2
p1
p2

Figure S1

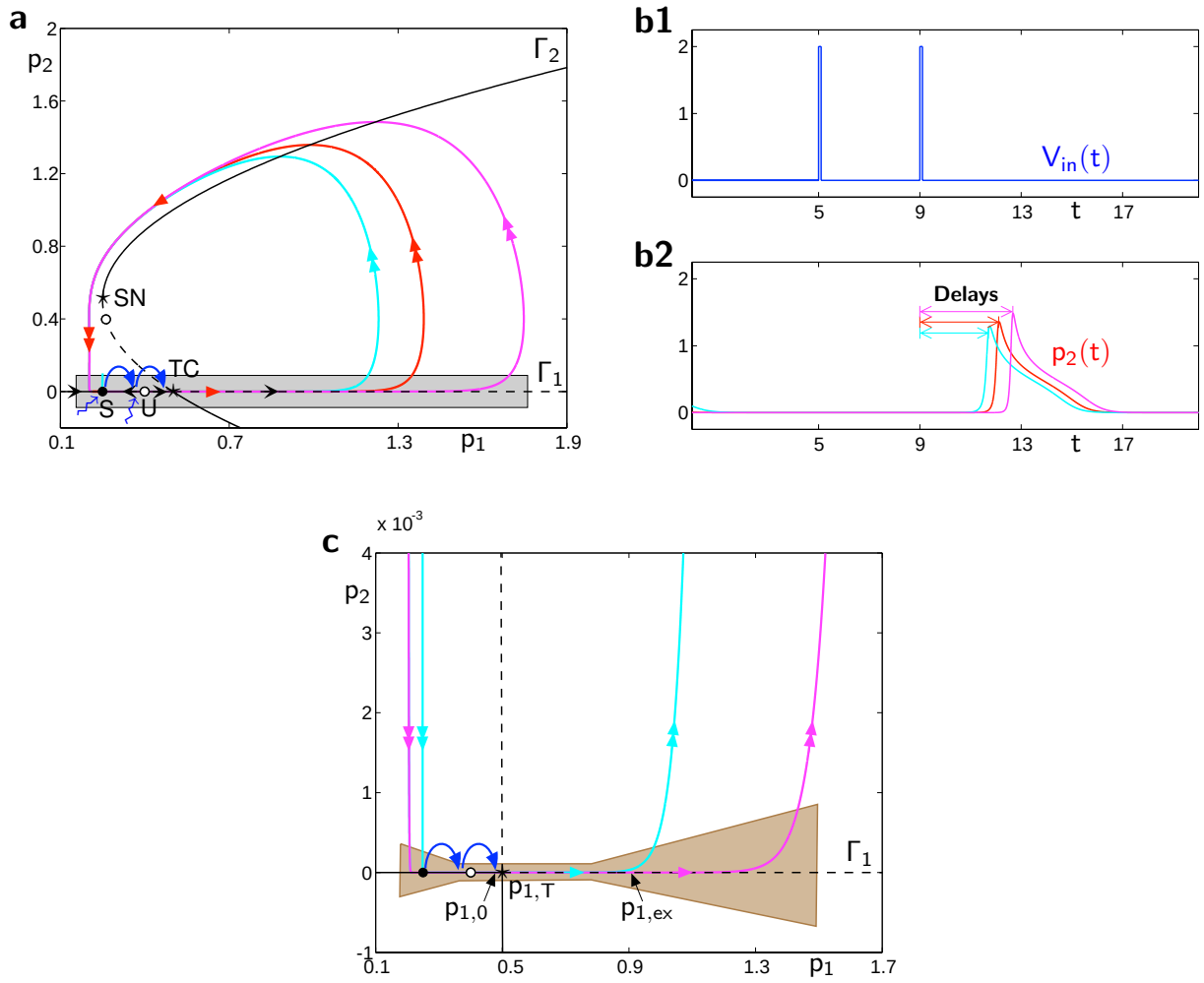
a
p2
Γ2
SN
TC
S
U
Γ1
p1
b1
Vin(t)
t
b2
Delays
p2(t)
t
c
x 10-3
p2
Γ1
p1,0
p1,T
p1,ex
p1

Figure S2

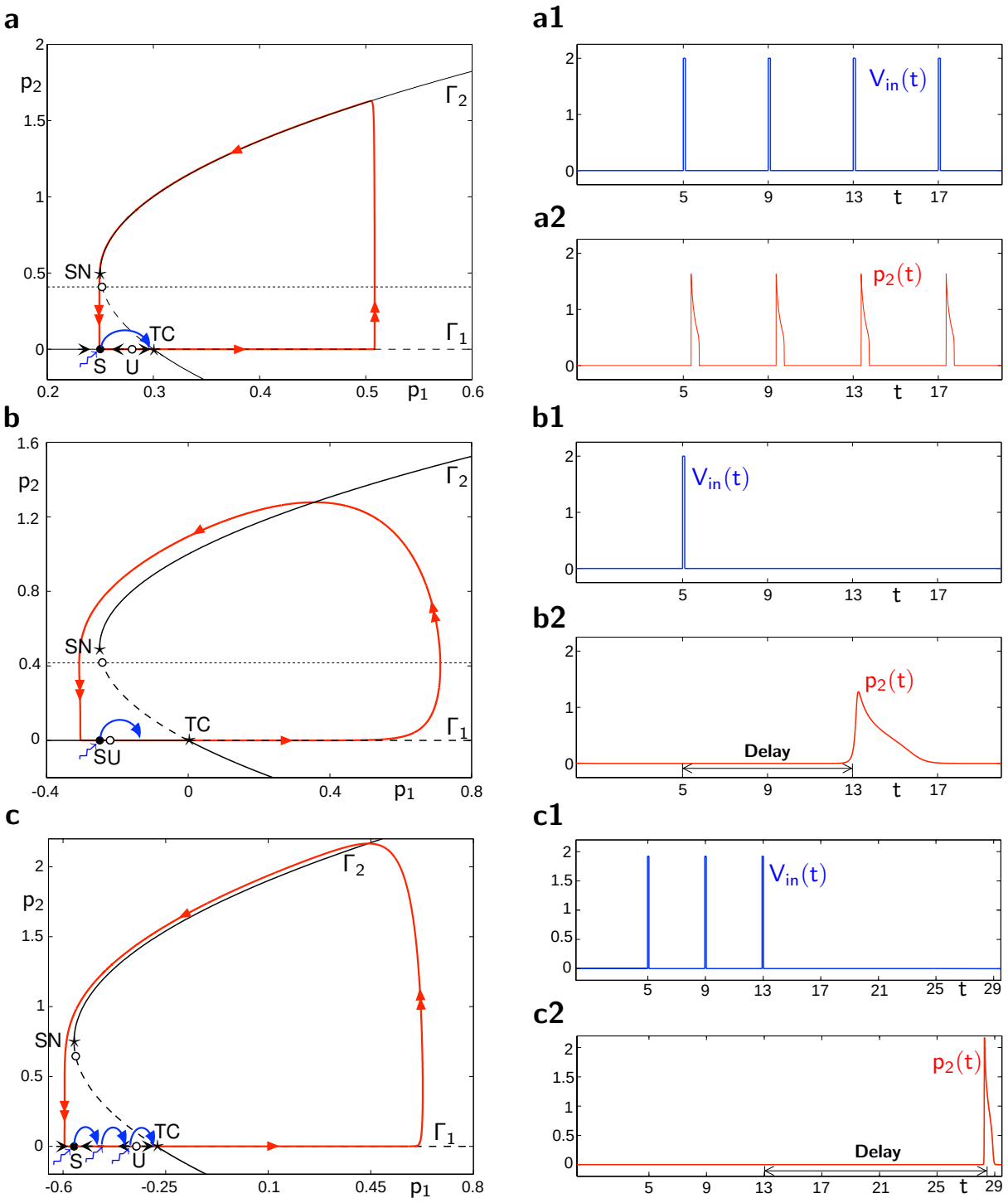
a
a1
a2
b
b1
b2
c
c1
c2
SN
TC
S
U
SU
Delay
p_2
p_1
Γ_1
Γ_2
$V_{in}(t)$
$p_2(t)$
t

Figure S3

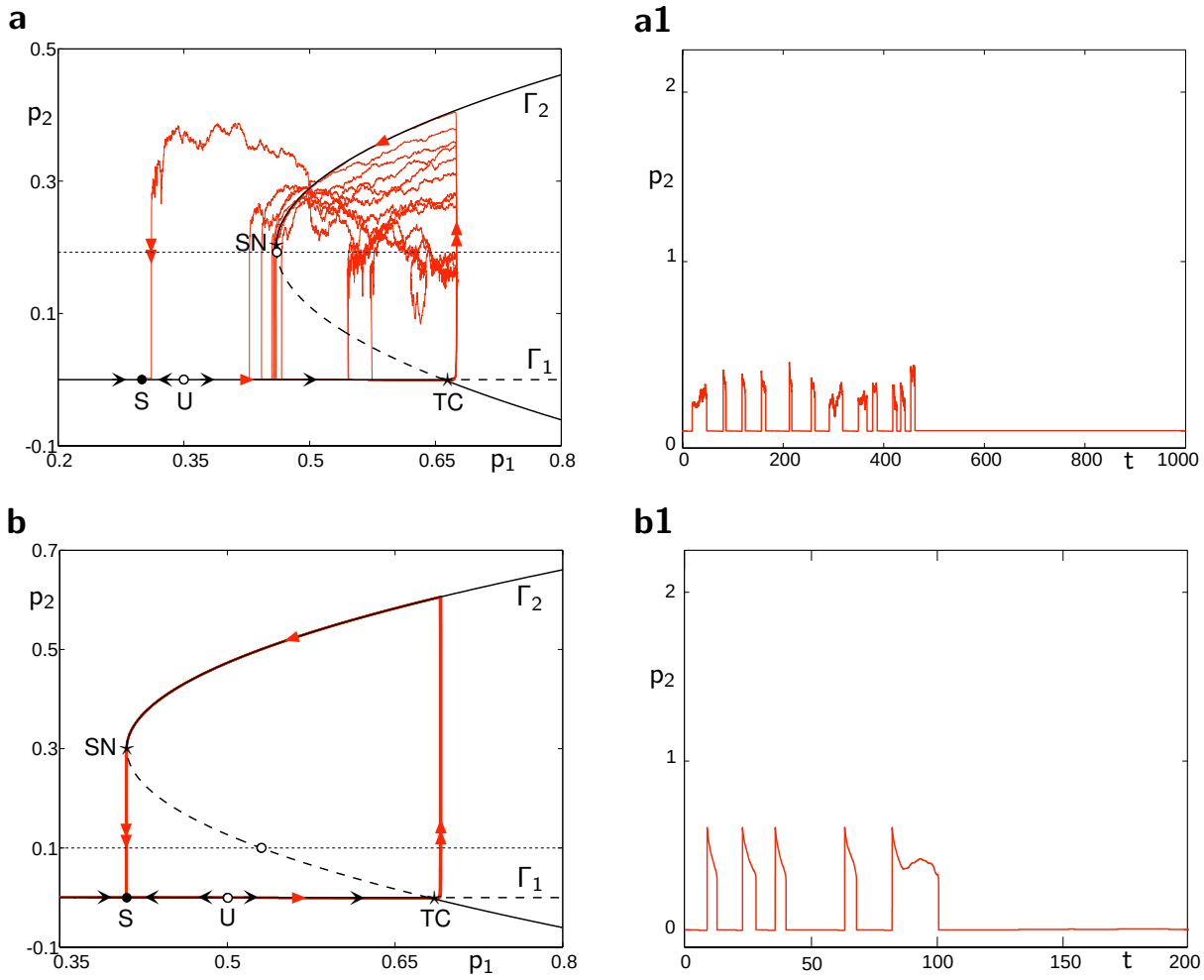

Figure S4

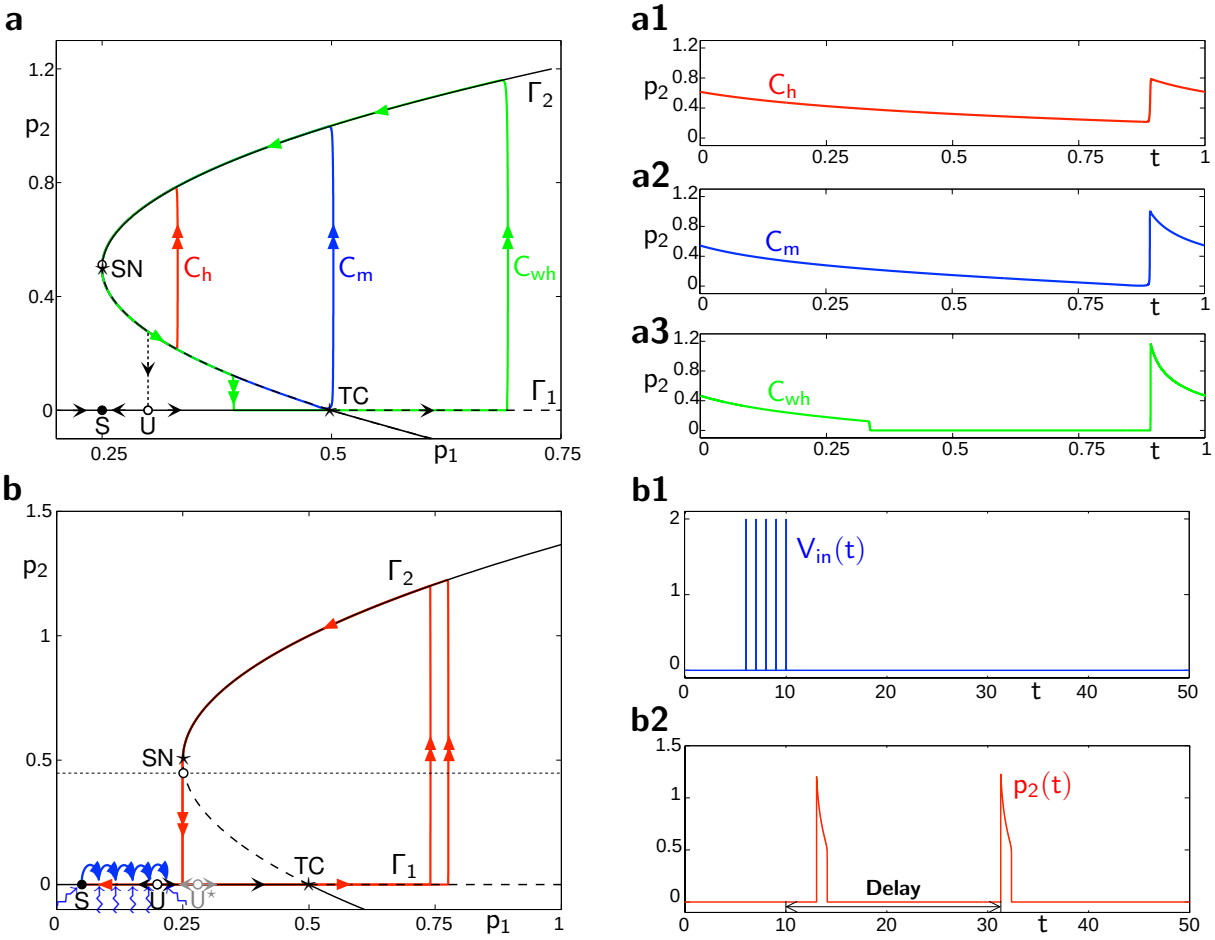
a
a1
a2
a3
b
b1
b2
SN
TC
S
U
C_h
C_m
C_{wh}
Γ_1
Γ_2
p_1
p_2
t
$V_{in}(t)$
$p_2(t)$
Delay

Figure S5

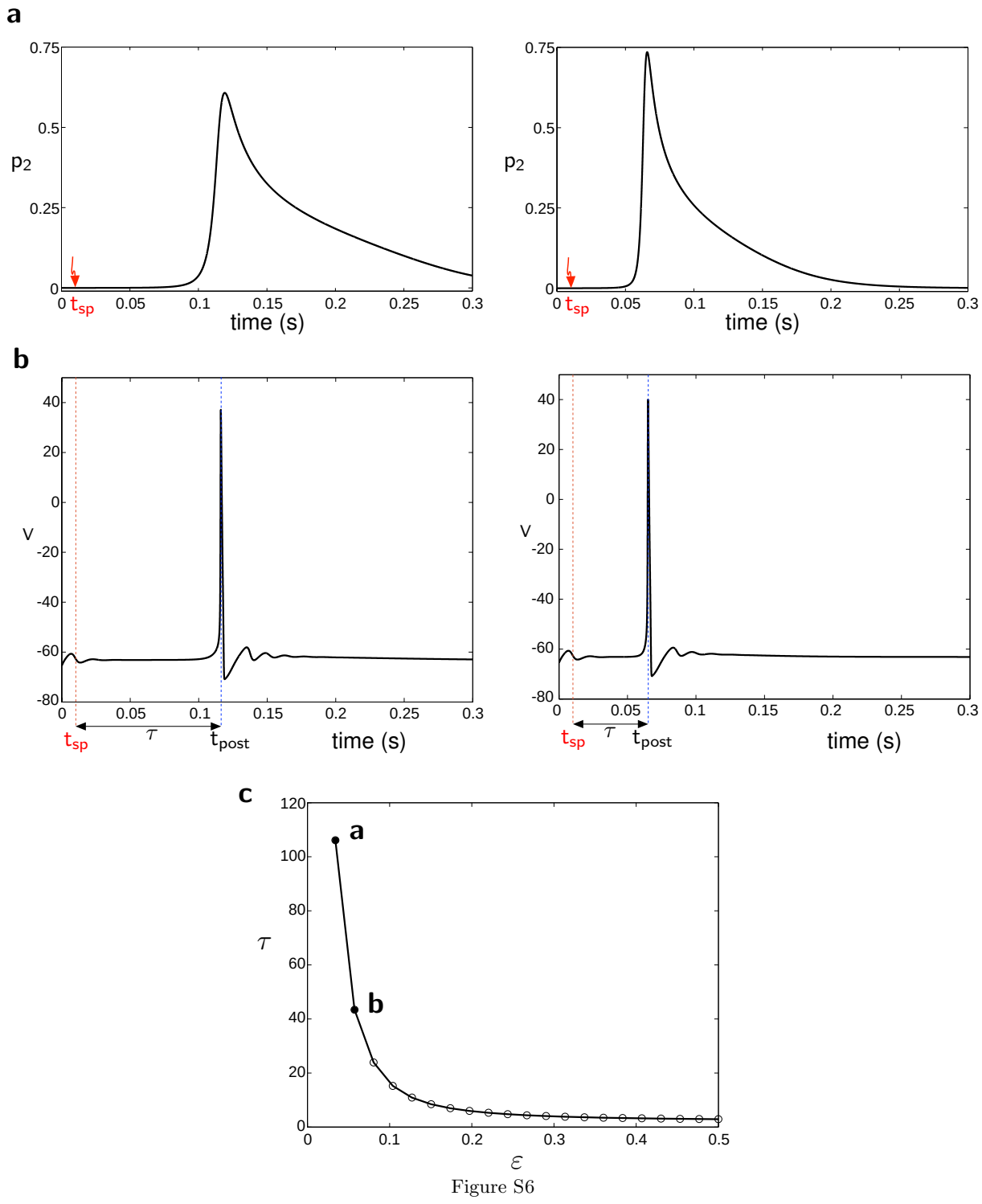
a
0.75
0.5
0.25
0
p2
0 tsp 0.05 0.1 0.15 0.2 0.25 0.3
time (s)
b
40
20
0
-20
-40
-60
-80
V
tsp
τ
tpost
time (s)
c
120
100
80
60
40
20
0
τ
a
b
0 0.1 0.2 0.3 0.4 0.5
ε

Figure S6

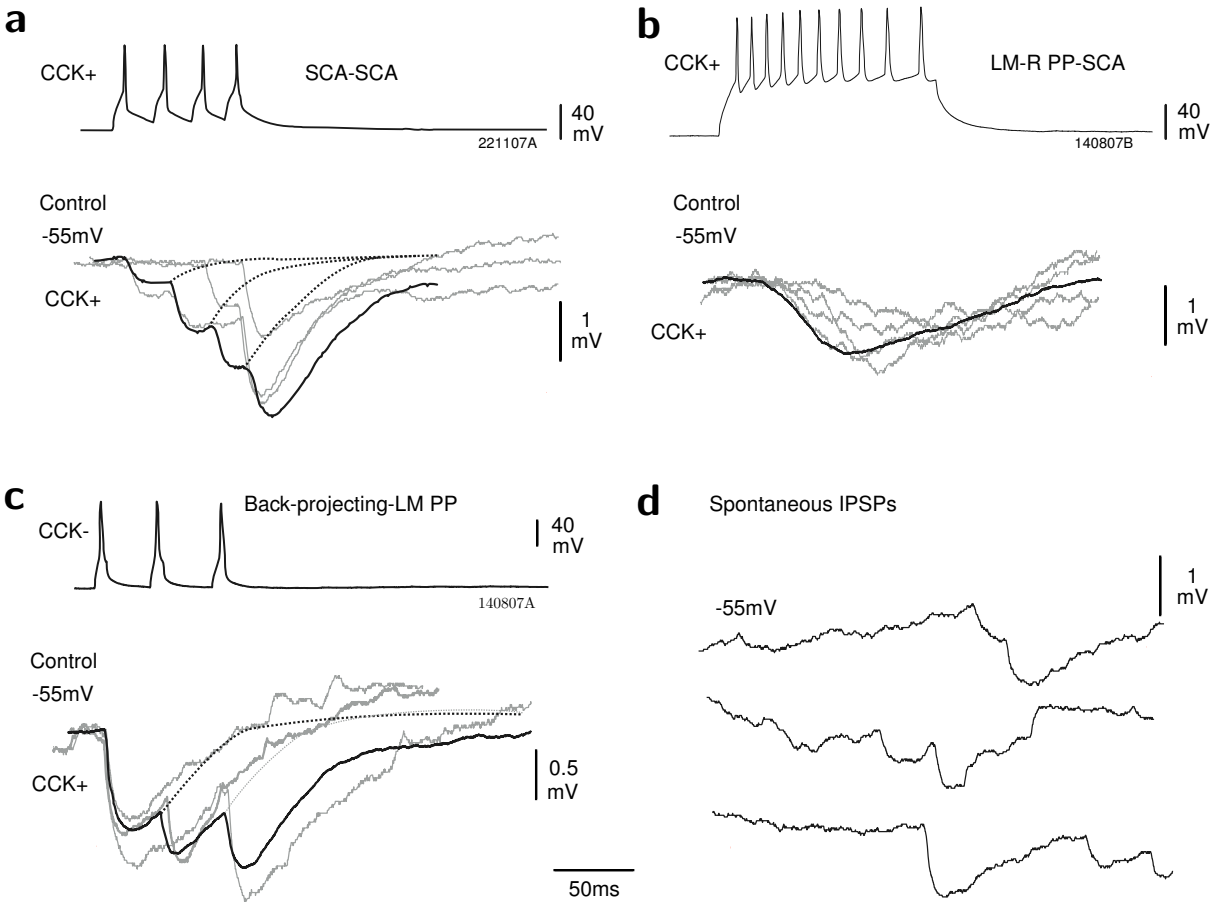
a
CCK+
SCA-SCA
40 mV
221107A
Control
-55mV
CCK+
1 mV
b
CCK+
LM-R PP-SCA
40 mV
140807B
Control
-55mV
CCK+
1 mV
c
CCK-
Back-projecting-LM PP
40 mV
140807A
Control
-55mV
CCK+
0.5 mV
50ms
d
Spontaneous IPSPs
1 mV
-55mV

Figure S7